Research in Astron. Astrophys. **2012** Vol. **12** No. **8**, 1107–1138
http://www.raa-journal.org *http://www.iop.org/journals/raa*

***R**esearch in*
***A**stronomy and*
***A**strophysics*

Solar-stellar astrophysics and dark matter

Sylvaine Turck-Chièze[1] and Ilídio Lopes[2,3]

[1] CEA/IRFU/Service d'Astrophysique, AIM, CE Saclay, 91191 Gif sur Yvette, France; *sylvaine.turck-chieze@cea.fr*
[2] Centro Multidisciplinar de Astrofísica, Instituto Superior Técnico, Universidade Técnica de Lisboa, Av. Rovisco Pais, 1049-001 Lisboa, Portugal; *ilidio.lopes@ist.utl.pt*
[3] Departamento de Física, Escola de Ciência e Tecnologia, Universidade de Évora, Colégio Luis António Verney, 7002-554 Évora, Portugal

Received 2012 July 2; accepted 2012 July 5

Abstract In this review, we recall how stars contribute to the search for dark matter and the specific role of the Sun. We describe a more complete picture of the solar interior that emerges from neutrino detections, gravity and acoustic mode measurements of the *Solar and Heliospheric Observatory* (*SOHO*) satellite, becoming a reference for the most common stars in the Universe. The Sun is a unique star in that we can observe directly the effect of dark matter. The absence of a signature related to Weakly Interacting Massive Particles (WIMPs) in its core disfavors a WIMP mass range below 12 GeV. We give arguments to continue this search on the Sun and other promising cases. We also examine another dark matter candidate, the sterile neutrino, and infer the limitations of the classical structural equations. Open questions on the young Sun, when planets formed, and on its present internal dynamics are finally discussed. Future directions are proposed for the next decade: a better description of the solar core, a generalization to stars coming from seismic missions and a better understanding of the dynamics of our galaxy which are all crucial keys for understanding dark matter.

Key words: stellar evolution: theory — elementary particles — helioseismology — dark matter — early solar-planet relationship

1 INTRODUCTION

Two major questions urgently need to be solved in astrophysics: Which matter forms the observed structures in the Universe? How does life emerge in the Universe? Faced with these questions, space missions of the last two decades have taken crucial opportunities to look at our Universe. Here we examine how our local environment informs us and helps to make progress in this area of knowledge.

In this review, we concentrate on studying the Sun and stars through seismology, representing a revolution in astrophysics. In the ESA-NASA *SOHO* mission (Domingo et al. 1995), launched and positioned around Lagrangian point L1 (where the Sun's gravity is equal to the Earth's one), a dozen instruments have continuously scrutinized the Sun for nearly 20 years to make progress on these questions. Soon COROT, SDO, PICARD and KEPLER will generalize our conclusion on the internal dynamical processes and on our understanding of the microscopic phenomena that we

directly study in the Sun's interior. We shall focus, in this review, on the deep core of the Sun where Weakly Interacting Massive Particles (WIMPs) could show a specific signature and on the radiative zone to enrich our study of another candidate, the sterile neutrino.

The recent developments in particle physics and cosmology have proposed various particle candidates to explain the nature of dark matter. These particles are at the forefront of improvements of modern astrophysics, so the Sun and stars can be studied as cosmological tools for modern cosmology.

The interest of studying the interactions of dark matter within stars is twofold: first, to identify which type of particle dark matter is made of, and second, to understand the physical mechanisms by which dark matter contributes to star formation. In the former, stars are used as a complementary cosmological tool to test the different dark matter candidates, providing in that way an alternative method to investigate the candidates proposed by modern theories of particle physics, or alternatively, to check the candidates detected by experiments used for direct or indirect dark matter searches. In the latter, the aim is to explore how dark matter contributes to structure formation in the Universe, including galaxies and the first generation of stars, not only by locally changing the gravitational field where stars are formed, but also by exploring how the possible interaction of dark matter with baryons changes the evolution of stars. Here, we will focus on the former topic.

Due to its proximity to Earth, the Sun is a unique stellar object in such an approach. Astronomers have collected large amounts of data on ground based observatories and in solar satellite missions. The solar surface is observed daily in all wavelengths of the electromagnetic spectrum. The Sun has also become a privileged plasma physics laboratory because its interior is probed by helioseismic instruments and solar neutrino detectors. Therefore, it is not surprising that the Sun has been an ideal target to test new ideas, not only directly related with the physical mechanisms that regulate stellar evolution, but also to check the validity of fundamental laws of physics. Furthermore, the successful use of the Sun to check physical processes has almost always been followed by similar studies in other stars. This strategy will continue in subsequent decades when new developments in observations and detectors are expected.

Last year, a review was dedicated to the interplay between neutrinos and seismology (Turck-Chièze & Couvidat 2011), focusing on how the two communities have improved their own research and their common understanding of the central core of the Sun. In the present paper, we describe in detail how the Sun's interior can be observed by using techniques from seismology. Even though the Sun is not a star where we may hope to find the strongest signature of dark matter, it is the only one where we can directly examine its effects using both neutrinos and seismic indicators from the radiative zone. So we give a quantitative description of the properties of the radiative zone that constitutes 98% of the mass of the Sun and is the region where effects from dark matter can be sought (Sect. 2). We recall properties of dark matter in a stellar context in Section 3, where the interactions of dark matter can be explored in stars, in particular in their core and we deduce the resulting limitations on the mass of WIMPs from current observations. We comment on the effects of dark matter on stellar evolution, in particular in our galaxy's center. Section 4 summarizes the open questions that emerge from the seismic observations, in particular on the formation of the Sun and planets. We finally propose some directions of research for the next generation of instruments and for new investigations.

2 THE INTERNAL SUN SEEN BY HELIOSEISMOLOGY

In stellar seismology, the Sun has a privileged status because it is observed both locally and globally. Thousands of modes have been detected, with the acoustic modes penetrating more or less deeply from the surface into the core and the gravity modes from the limit of the convective zone to the central region. So inversion methods have been derived to extract radial information from the surface to the center. By contrast, up to now other stars have only been observed globally with restricted

access to radial, dipolar and quadrupolar modes (except for deformed stars). Even though these modes are the most penetrating modes, only the Sun can benefit from all the information contained in the frequency of modes. In fact, gravity modes are slightly influenced by the physical processes occurring at the base of the convective zone and acoustic modes are strongly influenced by those processes at the near surface. This problem is avoided for the Sun by the knowledge of other modes that are more sensitive to these specific regions, so the solar core can really be scrutinized with a higher accuracy than the cores of other stars.

2.1 The Theoretical Framework

Solar or solar-like oscillations result from small adiabatic perturbations around the hydrostatic equilibrium of these stars. The perturbations generated by the granulation noise at the surface are very small, of the order of some $10^{-6} - 10^{-5}$ of the total luminosity of the star and with no exchange of energy due to the pulsation. Contrary to classical variable stars for which perturbations are strongly significant and non-adiabatic, the Sun-like pulsations do not affect the evolution of the star, as they occur in a free fall time of the order of one hour. Instead, the evolution of a star is determined by the transport of radiation which occurs in the Kelvin-Helmotz time, which is of the order of a million years in solar-like stars, so these two physical processes are decoupled.

More generally, stellar pulsations of Sun-like stars (including gravity modes and waves) can be written as a series of non-radial oscillations around a spherical structure of equilibrium and a variable *p* can be written in terms of spherical harmonics (Unno et al. 1989; Christensen-Dalsgaard & Berthomieu 1991):

$$p(r,\theta,\varphi,t) = p_0(r) + p'(r) Y_\ell^m(\theta,\varphi) \exp i\omega_{n,\ell,m} t,$$

p_0 is the variable at the equilibrium and the $\boldsymbol{\xi}$ displacement vector is defined as

$$\boldsymbol{\xi}(r,\theta,\varphi,t) = \left(\xi_{\rm r}(r), \xi_{\rm h}(r)\frac{\partial}{\partial\theta}, \xi_{\rm h}(r)\frac{\partial}{\sin\theta\partial\varphi}\right) Y_\ell^m(\theta,\varphi)\exp(i\omega_{n,\ell,m}t), \tag{1}$$

where $\xi_{\rm h} = 1/(\omega^2 r)[p^{'}/\rho + \Phi^{'}]$ is the horizontal displacement, $\Phi^{'}$ the perturbation in gravitational potential, $\omega_{n,l,m}$ the eigenfrequency, and ρ the gas density. The quantum numbers n, ℓ, and m are respectively the radial order (number of nodes along the radius), the degree (the total horizontal wave number at the surface is $k_{\rm h} \sim L/R_\odot$, with $L = \sqrt{\ell(\ell+1)}$), and the azimuthal order (number of nodes along the equator with $|m| \leq \ell$).

Restricting the phenomenon to adiabatic oscillations within the Cowling approximation ($\Phi^{'}$ neglected) and considering only small radial wavelengths compared to $R_\odot$, the 4th-order system of equations is reduced to second-order wave equations, with the following dispersion relation

$$k_{\rm r}^2 = \frac{1}{c_{\rm s}^2}\left[F_{\rm l}^2\left(\frac{N^2}{\omega_{n,\ell,m}^2} - 1\right) + \omega_{n,\ell,m}^2 - \omega_c^2\right], \tag{2}$$

where the squared norm of the wave vector is written as the sum of a radial and a horizontal component $|\boldsymbol{k}| = k_{\rm r}^2 + k_{\rm h}^2$, $k_{\rm h}^2 = F_{\rm l}^2/c_{\rm s}^2$ is the horizontal wave number, $F_{\rm l}^2 = L^2 c_{\rm s}^2/r^2$ is the Lamb frequency, $N^2 = g[1/\Gamma_1 d\ln p/dr - d\ln\rho/dr]$ is the Brunt-Väisälä frequency, $\omega_c^2 = c_{\rm s}^2(1 - 2dH_\rho/dr)/4H_\rho^2$ is the acoustic cut-off frequency (~ 5.8 mHz), $H_\rho^{-1} = -d\ln\rho/dr$ is the density scale height, Γ_1 is the adiabatic exponent, and $c_{\rm s}^2 = \Gamma_1 p/\rho$ is the sound speed.

The mode frequency $\nu_{n,\ell,m}$ is labeled by its order n (number of nodes along the radius) and degree ℓ (number of reflections at the surface). A theoretical prediction of the frequency is necessary to identify them, so the model frequencies are always calculated in parallel and compared to the observed frequencies (see Table 1). In the presence of internal rotation and a magnetic field, the ℓ

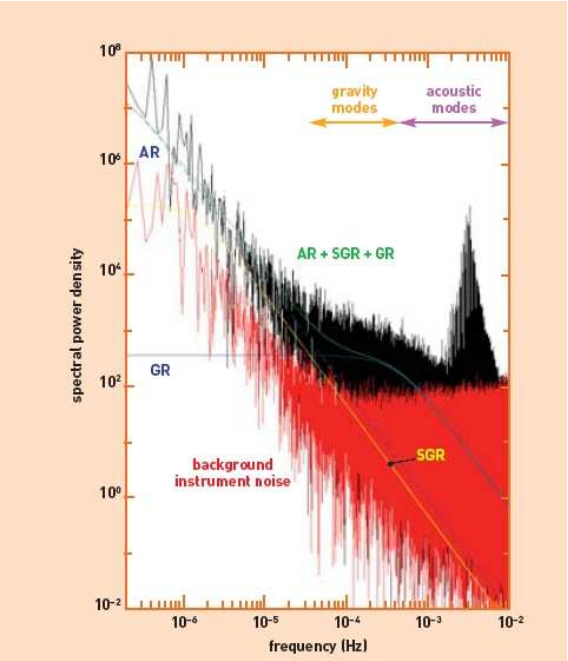

Fig. 1 Fourier transform power spectrum of the solar GOLF residual velocity time series, showing the respective ranges of gravity and acoustic modes together with the contribution of the solar noise due to the activity of the Sun (granulation + active regions). From Turck-Chièze et al. (2004a).

component is split into $2\ell + 1$ azimuthal orders m, or even more, if the magnetic field is important and observed with a different axis. In fact, due to the rotation of the star, the travel time of the modes differs depending on if their displacement follows the rotation of the star or if it follows the opposite direction. Furthermore, in Sun-like stars, the rotation and magnetic field present in the stellar interior produce variations in $\nu_{n,\ell,m}$ of the order of a few tenths of μHz and a few nHz, respectively.

2.2 The Low Degree Modes Observed by *SOHO*

Acoustic, gravity and mixed modes are now detected in a lot of solar-like stars. The first are generated by convective motion at the surface and sensitive to the pressure gradient, while gravity modes are sensitive to the gravity and probably excited by the turbulent motions at the base of the convective zone. Mixed modes couple the specificity of the two previous categories. Altogether they represent different types of information about the Sun's interior (Aerts et al. 2010).

Figure 1 shows the global power spectrum of the solar modes obtained with the Global Oscillations at Low Frequencies (GOLF) instrument aboard *SOHO* (Gabriel et al. 1995; Turck-Chièze et al. 2004a). This instrument, looking to the Sun as a star, has shown its capability to detect both acoustic modes of low amplitude and some gravity modes due to its Doppler shift velocity measurement of the sodium line, located between $300 - 500$ km above the solar surface where the turbulent solar noise is strongly reduced. Its performances are also due to its very low intrinsic instrumental noise (in red on the figure) that permits a search for gravity modes down to 5×10^{-5} Hz.

Figure 2(a) shows the Doppler velocity measurements of the GOLF instrument during the first hours after it began collecting scientific data in 1996 January. One observes the velocity between the Sun and the spacecraft including gravitational redshift (GRS). The space measurement avoids the

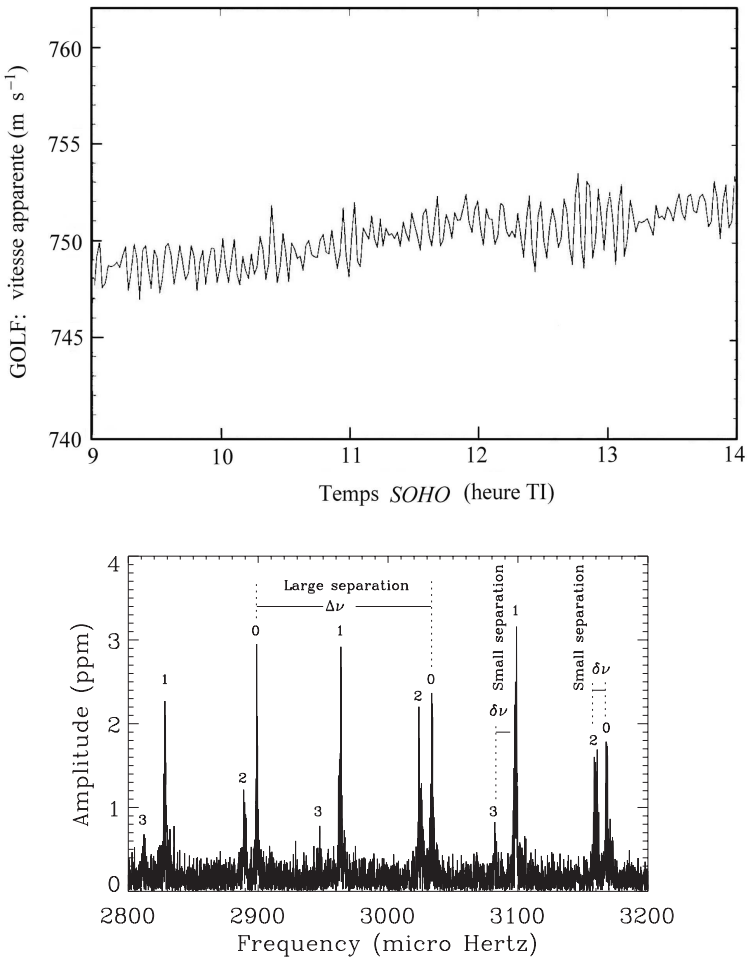

Fig. 2 (a) Historical spectrum of the GOLF Doppler velocity measurements showing the first 14 hours of 1996 January 15. One sees, superimposed on the mean velocity, the 5 mn acoustic oscillations (about 3.3 mHz) and the stochastic character of their excitation. (b) Enlarged view of the maximum of the power spectrum for a solar-like star to illustrate the fact that the acoustic modes are spaced in frequencies and show the specific characteristics of the different degrees described in Eqs. (3) and (4).

large variation of velocity during the day as observed on Earth; *SOHO* evolves in an orbit around the L1 Lagrange point, in permanent view toward the Sun. Superimposed on this mean velocity, the 5 minute oscillation period (the acoustic modes have their maximum amplitude near 3.3 mHz as shown in Fig. 1) clearly exhibits the stochastic character of the granulation excitation. This time series has been followed continuously since 1995 and the Fourier transform is performed on the residual after subtracting the main component (Sun-spacecraft velocity) plus sunspots (see García et al. 2005). After two years of integration, one gets the Fourier transform spectrum shown in Figure 1 but the integration is desired on a longer series, up to the whole mission (20 years) in order to reduce the white noise in comparison with the useful periodic signals that appear as Lorentzian peaks for which

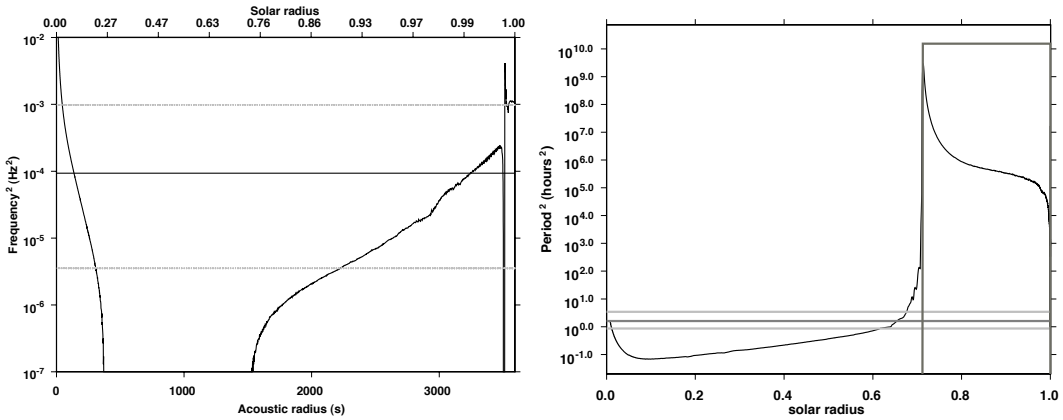

Fig. 3 *Left*: Squared acoustic potential for the mode $\ell = 1$ and $\nu = 1500$ μHz (*black line*). The gray dotted lines correspond respectively to the dipole modes at 5000 and 300 μHz. *Right*: Squared gravity potential. The black line corresponds to the gravity mode $\ell = 2$, $n = -3$ (*black line*). The gray lines correspond to the band $150 - 400$ μHz. From Turck-Chièze et al. (2004a).

the width decreases with frequency (the longevity of the modes increases at high period) (Gelly et al. 2002).

2.2.1 The solar acoustic modes

The first detections of the acoustic modes appeared thirty years ago (Claverie et al. 1979; Grec et al. 1980). The orders of the same degree present a nearly regularly spaced comb pattern in frequency (Fig. 2(b)) following an asymptotic behavior given below, where the phase shift α is largely dependent on the physics of the subsurface and of the EOS of helium and hydrogen

$$\nu_{n,\ell} = \Big(n + \frac{\ell}{2} + \frac{1}{4} + \alpha\Big)\Delta\nu\,, \quad \text{where } \Delta\nu = \Big[2\int_0^R \frac{dr}{c}\Big]^{-1}. \tag{3}$$

The relation between $\Delta\nu$ and the sound speed c is extremely useful to label the frequencies. The variation of α with frequency due to the physics of the substructure can be isolated for the Sun and Sun-like stars (Lopes & Gough 2001). A second quantity, the small separation, i.e. the distance between successive orders and degrees differing by two, is also useful for solar-like stars due to its increased sensitivity to the cores of stars

$$\delta\nu_{n,\ell} = \nu_{n,\ell} - \nu_{n-1,\ell+2} \approx -(4\ell+6)\frac{\Delta\nu}{4\pi^2\nu_{n,\ell}}\int_0^R \frac{dc}{r}\frac{dr}{r}. \tag{4}$$

By contrast, the large difference is mainly sensitive to the layers below the surface. The two quantities $\Delta\nu$ and $\delta\nu$ allow researchers to place the star in the seismic diagram (Christensen-Dalsgaard 2004) from which one deduces an estimate of its mass and age. Nevertheless, it is a first approximation. A generalization at second order has been developed for both high ℓ (Vorontsov 1991) and low degree modes (Lopes & Turck-Chieze 1994) that find better evidence about the role of the sub surface layers and of the gravity in the core when one can only measure low degree modes; this will be used soon for solar-like stars.

By chance, the Sun is also observed locally, thanks to the MDI (Michelson Doppler Imager) aboard *SOHO* and to the GONG network (Scherrer et al. 1995; Harvey et al. 1996), so a large number of acoustic modes are available for degrees ℓ= 0 to 300, and potentially more. An inversion procedure is then possible from which one deduces the radial profiles of different quantities (see below). Consequently one can very precisely explore the information contained in the mode frequencies, in particular the sensitivity of the acoustic mode frequency to both the sub surface layers and the core of the Sun, as shown in the left panel of Figure 3.

Above 2.5 mHz, the solar low degree acoustic frequencies vary with the 11 year solar cycle (Chaplin et al. 2007; Salabert et al. 2009). Section 2.5 describes the origin of this variability. The variation is not larger than 0.5 μHz, but needs to be taken into account properly as the sound speed of the surface layers is significantly smaller than the sound speed of the center (see Table 3). The left panel of Figure 3 shows that a low degree acoustic mode spends at least half its propagation time in the convective zone (2% in mass) so that region (in particular the ionization zones) has to be studied precisely if one would like to obtain quality information about the deep interior (central region).

Figure 4 compares the order of magnitude of the different contributions to the frequency, in particular the region below $R < 0.2R_{\odot}$.

Figure 4(a) (García et al. 2001) shows the internal turning point of the low degree modes (ℓ = 0, 1, 2) for different orders. The higher the order ($N = 30$) and the lower the degree ($l = 0$), the more the mode penetrates into the deep core, but the figure also shows that a variation of the sound speed by 0.5% or 1% in the core could be the same size as the error bar. So a lot of caution is required to extract any information from this region of the Sun.

Figure 4(b) (Couvidat et al. 2003b) completes this demonstration in showing the frequency error bars after 1 year of observation (top figure), then after 5 years for all the modes (middle) and in the last plot for modes below $n = 17$ (bottom) (Couvidat et al. 2003b). This comparison shows that the low order modes, even though they penetrate less deeply into the core, contain invaluable information as they are much better determined. In fact, the width of the modes decreases with frequency so if they are visible (their amplitude is smaller, see Fig. 1) they represent the best information on the deep interior; this demonstrates the superiority of the space measurements over the network measurements which are also polluted in this range of frequencies (below about 2.5 mHz) by the Earth's atmospheric noise. Moreover, the low order frequencies are not polluted by the solar cycle's variability so they allow the extraction of a good radial profile of the sound speed as deep as possible.

Table 1 gives the list of frequencies detected by GOLF at the solar activity minimum for modes greater than 2.5 mHz. Smaller frequencies of the low order modes are obtained after 5 years of integration. Of course the visibility of GOLF is maximal for radial modes and the width of the modes decreases with frequency, so the accuracy is higher when the frequency decreases. The ℓ = 3 modes are only partly determined with GOLF and the missing values are obtained from MDI together with the higher ℓ modes, which are extremely important for extracting information from the surface to the center.

2.2.2 The solar gravity modes

The solar gravity modes have a small amplitude and are even more difficult to detect than the low frequency acoustic modes because they are evanescent in the convective zone. Their detection supposes a low solar granulation noise (see Fig. 1) and no pollution from the Earth's atmosphere below 2 mHz; these two points exclude any detection from the ground and make their detection difficult by intensity measurement in space (Fig. 11). Up to now, the GOLF instrument appears to be the most well adapted for this search (Turck-Chièze et al. 2004a; García et al. 2007; Turck-Chièze & Couvidat 2011) due to its excellent detection capability, see also Section 4.3. Surprisingly the mixed modes have appeared easier to detect in other solar-like stars (in fact slightly more massive). One can understand this fact in considering that the maximum amplitude of the acoustic modes increases

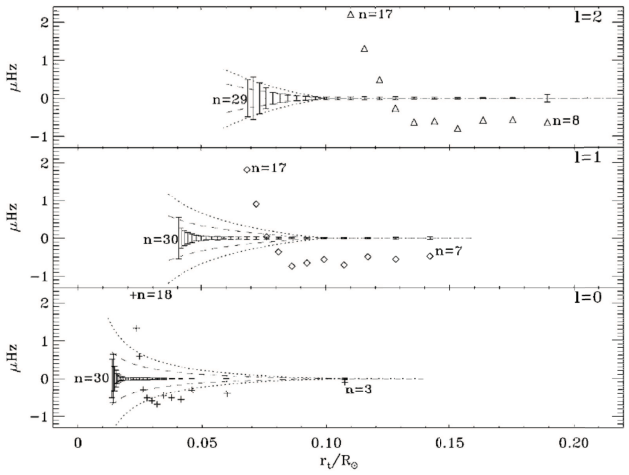

(a)

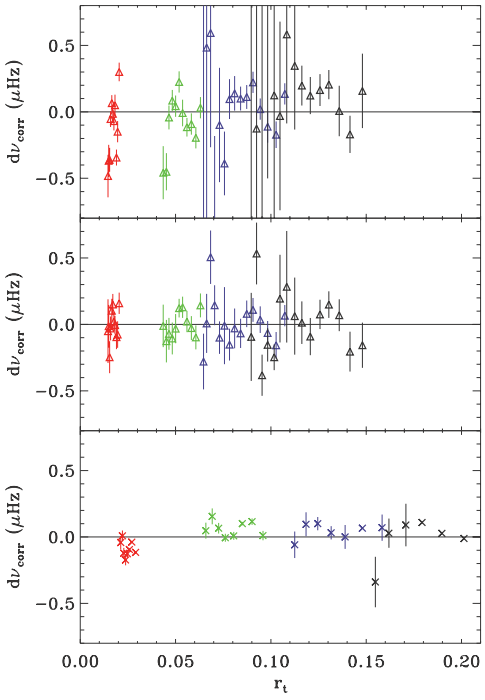

(b)

Fig. 4 (a) Observational error bars of the ℓ = 0, 1, and 2 p-mode frequencies compared to the difference, $\delta\nu$, between their measured frequencies and the theoretical ones (*crosses*, *diamonds and triangles*) and with the frequency uncertainty due to a modification of 1% (*dotted lines*) or 0.5 % (*dashed lines*) of the sound speed below 0.1 $R_\odot$ as a function of their inner turning point $r_t = c_t L/\omega_{\ell,n}$ where $L = \ell + 1/2$ (Lopes & Turck-Chieze 1994). The order n of the modes is written in the plot: 3 and 30 for ℓ = 0, 7 and 30 for ℓ = 1, and 8 and 29 for ℓ = 2. The difference $\delta\nu$ for the modes ℓ = 0, $n > 18$ and ℓ = 1 and 2, $n > 17$ are off the scale. From García et al. (2001). (b) Change of frequencies and respective error bars of global acoustic modes obtained after one year of GOLF observation (*upper panel*) for radial modes in red, dipolar modes (*green*), quadrupolar modes (*blue*) and $\ell = 3$ (*black*) as a function of their respective turning points. The same for these modes after 5 years of measurements. From Couvidat et al. (2003b).

Table 1 Global mode frequencies expressed in μHz obtained by the GOLF instrument. This table consists of observations near the minimum in the solar cycle between 1996 April 16 and 1998 June 24 for frequencies above 2.5 mHz (Gelly et al. 2002). Below, the acoustic mode frequencies are from Bertello et al. (2000); García et al. (2001). The gravity mode frequencies are derived from the frequency spectrum obtained after 10 years of observation (García et al. 2011; Turck-Chièze et al. 2012). The signal around 220 μHz is permanently visible both in GOLF and VIRGO (Turck-Chièze et al. 2004a; Jiménez & García 2009).

n	$\ell=0$	error	$\ell=1$	error	$\ell=2$	error	$\ell=3$	error
–10	–	–	62.50	0.05	–	–	–	–
–9	–	–	68.34	0.05	–	–	–	–
–8	–	–	75.39	0.05	–	–	–	–
–6	–	–	95.34	0.05	–	–	–	–
–5	–	–	109.40	0.05	–	–	–	–
–4	–	–	127.74	0.05	–	–	–	–
–3	–	–	–	–	220.1– 220.7	?	–	–
1	258.60	0.030	–	–	–	–	–	–
3	535.75	0.010	–	–	–	–	–	–
5	825.23	0.030	–	–	–	–	–	–
6	972.612	0.005	1039.465	0.003	–	–	–	–
7	–	–	1185.60	0.05	–	–	–	–
8	1263.215	0.01	1329.63	0.01	1394.680	0.01	–	–
9	1407.49	0.01	1472.857	0.02	1535.865	0.006	–	–
10	1548.304	0.009	1612.746	0.011	1674.534	0.013	1729.74	0.02
11	1686.581	0.18	1749.290	0.010	1810.349	0.015	1865.29	0.03
12	1822.196	0.018	1885.113	0.015	1945.80	0.02	2001.24	0.04
13	1957.43	0.02	2020.84	0.02	2082.15	0.02	2137.80	0.03
14	2093.53	0.02	2156.83	0.02	2217.69	0.03	2273.57	0.04
15	2228.84	0.02	2292.09	0.03	2352.29	0.03	2407.65	0.05
16	2362.83	0.03	2425.61	0.03	2485.86	0.03	2541.55	0.07
17	2496.26	0.02	2559.20	0.04	2619.64	0.04	2676.22	0.06
18	2629.72	0.04	2693.38	0.04	2754.39	0.04	2811.48	0.06
19	2764.17	0.04	2828.15	0.04	2889.57	0.04	2947.00	0.05
20	2899.05	0.04	2963.29	0.04	3024.710	0.05	3082.24	0.06
21	3033.77	0.03	3098.14	0.05	3159.84	0.04	3217.84	0.06
22	3168.65	0.04	3233.10	0.04	3295.06	0.05	3353.54	0.10
23	3303.39	0.04	3368.48	0.06	3430.75	0.09	3489.51	0.09
24	3439.02	0.05	3503.89	0.07	3566.68	0.12	3625.99	0.20
25	3574.68	0.09	3640.22	0.08	3702.84	0.14	3763.11	0.32
26	3710.75	0.12	3776.40	0.11	3839.11	0.21	3900.44	0.48
27	3846.79	0.17	3913.03	0.13	3976.41	0.26	4037.02	0.60
28	3984.45	0.22	4049.91	0.16	4114.13	0.29	4174.46	0.96
29	4121.30	0.34	4187.18	0.20	4249.90	0.33	4312.98	1.04
30	4259.77	0.34	4325.71	0.25	4389.30	0.37	4454.11	1.83
31	4397.43	0.60	4462.00	0.39	4525.71	0.651	–	–
32	4534.65	0.701	4599.03	0.33	4663.86	0.651	–	–
33	4675.52	0.951	4737.61	0.40	4806.45	1.701	–	–
34	4808.60	3.961	4875.75	0.59	4944.88	0.811	–	–
35	4955.59	2.311	5016.82	0.82	–	–		
36	5086.18	0.981	5157.08	1.10	–	–		

with mass (Verner et al. 2011)

$$\frac{A_{\max}}{A_{\max,\odot}} = \Big(\frac{L/L_\odot}{M/M_\odot}\Big)^s \Big(\frac{T_{\rm eff}}{T_{\rm eff,\odot}}\Big)^{0.5}, \quad \text{where} \quad s = -0.64 - 1.18\Big(\frac{T_{\rm eff} - T_{\rm eff,\odot}}{T_{\rm eff,\odot}}\Big) \tag{5}$$

and that the size of the convective zone diminishes when the mass increases.

The *SOHO* satellite opens a real opportunity for the detection of solar gravity modes compared to previous ground-based efforts and the quality of GOLF is due to its exceptional low background

instrumental noise at low frequency (Fig. 1). This property comes from the two photomultiplier detectors equipped with an electronic device specifically designed to produce noise that always stays lower than the statistical noise chosen as low as 2×10^{-4}; this requirement has been reached in tracking and avoids any source of noise that appeared greater than such a specification before launch (Gabriel et al. 1995).

The lifetime of the gravity modes increases as the frequency decreases, so their detection benefits from a long and continuous space mission. We have analyzed the first 5 years of integrated signal, then 10 and soon more than 15 years. Two directions of investigation have been adopted following the gravity mode properties described in Provost & Berthomieu (1986); Provost et al. (2000).

The first was to look for mixed modes because they are the most informative ones in terms of both the core's dynamics and the base of the convective zone (Mathur et al. 2007) as their cavity is the largest, see the right panel in Figure 3. Several patterns have been studied, in particular around 220 μHz that could be attributed to an $\ell = 2$, $n = -3$ mode (Turck-Chièze et al. 2004a; Jiménez & García 2009), but the strict identification of the components remains difficult due to several properties of these modes that were not known before: (1) the central frequency can be perturbed by the rotation of the core, (2) the patterns are not strictly stable over several years; this is contrary to what was previously believed, since this variability is certainly due to the instability of the base of the convective zone (Dintrans et al. 2005), (3) one cannot exclude the possibility that the core is rotating along a different axis than the rest of the radiative zone, so the power could be distributed between more components of a mode than for acoustic modes, which leads to a more complex identification. A longer integration could benefit observations of this range of frequency, if the ageing of the instrument does not deteriorate *SOHO's* ability to acquire information too much; after nearly 20 years in space, the counting rate has been reduced by a factor 10, from 6×10^6 to $5{\times}10^5$ photons s^{-1} per detector.

The second approach was to discover a signature of the asymptotic character of the frequencies below 130 μHz. These modes must appear practically equidistantly spaced in period (Tassoul 1980; Provost & Berthomieu 1986)

$$P_{n,\ell} = \frac{P_0}{2\sqrt{\ell(\ell+1)}}(2n + \ell + \phi) + \frac{P_0}{P_{n,\ell}} W_\ell, \tag{6}$$

with

$$P_0 = 2\pi^2 \left(\int_0^{r_c} \frac{N}{r} dr \right)^{-1} \quad \text{and} \quad W_l = V_1 + \frac{V_2}{\ell(\ell+1)}, \tag{7}$$

where N is the Brunt Väissälä frequency defined by

$$N^2 = g \left[\frac{1}{\Gamma_1} \Big(\frac{d}{dr} \log\, P(r) - \frac{d}{dr} \log\, \rho(r) \Big) \right],$$

where ϕ is a phase factor that depends on n and ℓ. V_1 depends on N and V_2 is a complex term, and both translate the small departure from pure equidistance between mode periods. The first study has avoided the problem of identification of individual peaks in summing the power spectrum between 25 to 140 μHz. In looking at the periodigram spectrum, the power of about 20 modes of the same degree is visible with the advantage of maximizing the signal to noise ratio. This work contributes evidence about the detection of dipole modes with more than a 99.7% confidence level and their sensitivity to a high rotation rate in the core (García et al. 2007). A longer series has reached a confidence level of at least 99.99% (García et al. 2008). The next step has consisted of looking locally at the power spectrum. The pattern of components ($m = \pm 1$) for six individual dipole modes appear on more than 10 years of integrated signal, and their centroid value (corresponding to $m = 0$) has been introduced in Table 1. Their splitting values are consistent with a rapid increase of the core's rotation (García et al. 2011). The frequencies of these dipole modes agree remarkably well with the predictions of

Table 2 Observed solar sound speed profile obtained by GOLF and MDI instruments located aboard *SOHO*. From Turck-Chièze et al. (2001); Couvidat et al. (2003b).

$r/R_\odot$	Sound speed (m s^{-1})	$r/R_\odot$	Sound speed (m s^{-1})
0.079 ± 0.03	510 540.0 ± 155.0	0.538 ± 0.015	285 924.0 ± 21.0
0.081 ± 0.03	510 426.0 ± 141.0	0.550 ± 0.015	281 887.0 ± 21.0
0.084 ± 0.03	510168.0 ± 120.0	0.563 ± 0.014	277 529.0 ± 20.0
0.089 ± 0.03	509 509.0 ± 92.0	0.575± 0.014	273 551.0 ± 20.0
0.099 ± 0.035	507 787.0 ± 70.0	0.588± 0.014	269 299.0 ± 19.0
0.112 ± 0.033	504 228.0 ± 68.0	0.60 ± 0.0135	265 404.0 ± 19.0
0.126 ± 0.034	498 956.0 ± 76.0	0.612± 0.013	261 512.0 ± 18.0
0.138 ± 0.033	493 352.0 ± 76.0	0.625 ± 0.013	257 270.0 ± 18.0
0.150 ± 0.033	486 888.0 ± 67.0	0.637 ± 0.013	253 311.0 ± 18.0
0.163 ± 0.032	479 133.0 ± 61.0	0.650 ± 0.0126	248 938.0 ± 17.0
0.177 ± 0.030	470 169.0 ± 60.0	0.663 ± 0.0124	244 443.0 ± 17.0
0.188 ± 0.029	462 834.0 ± 58.0	0.675 ± 0.012	240 092.0 ± 17.0
0.200 ± 0.028	454 688.0 ± 53.0	0.687 ± 0.012	235 438.0 ± 16.0
0.213 ± 0.028	445 817.0 ± 50.0	0.700 ± 0.012	229 966.0 ± 16.0
0.226 ± 0.027	436 984.0 ± 49.0	0.712 ± 0.011	224 352.0 ± 16.0
0.238 ± 0.026	428 924.0 ± 47.0	0.725 ± 0.011	217 217.0 ± 15.0
0.250 ± 0.025	420 976.0 ± 44.0	0.737 ± 0.011	210 674.0 ± 15.0
0.263 ± 0.024	412 524.0 ± 44.0	0.750 ± 0.010	203 616.0 ± 15.0
0.275 ± 0.024	404 921.0 ± 42.0	0.762 ± 0.010	197 074.0 ± 15.0
0.288 ± 0.023	396 956.0 ± 40.0	0.775 ± 0.010	189952.0 ± 14.0
0.300 ± 0.025	389 874.0 ± 39.0	0.787 ± 0.009	183 359.0 ± 14.0
0.313 ± 0.022	382 475.0 ± 37.0	0.800 ± 0.009	176 163.0 ± 13.0
0.325 ± 0.021	375 883.0 ± 36.0	0.812 ± 0.009	169 427.0 ± 13.0
0.338 ± 0.021	368 980.0 ± 35.0	0.825 ± 0.0085	162 080.0 ± 13.0
0.350 ± 0.020	362 830.0 ± 33.0	0.837 ± 0.008	155 168.0 ± 12.5
0.363 ± 0.020	356 382.0 ± 32.0	0.850 ± 0.008	147 567.0 ± 12.0
0.375 ± 0.019	350 610.0 ± 31.0	0.862 ± 0.0075	140 368.0 ± 12.0
0.388 ± 0.019	344 526.0 ± 30.0	0.875 ± 0.007	132 375.0 ± 11.0
0.400 ± 0.019	339 078.0 ± 29.0	0.887 ± 0.007	124 742.0 ± 11.0
0.413 ± 0.018	333 374.0 ± 28.0	0.900 ± 0.007	116 158.0 ± 10.0
0.425 ± 0.017	328 290.0 ± 27.0	0.912 ± 0.006	107 872.0 ± 10.0
0.437 ± 0.017	323 333.0± 26.0	0.925 ± 0.006	98 348.0 ± 9.0
0.450 ± 0.017	318 084.0 ± 26.0	0.937 ± 0.006	88 936.0 ± 10.0
0.462 ± 0.017	313 373.0 ± 25.0	0.950 ± 0.005	77 730.0 ± 9.0
0.475 ± 0.016	308 426.0 ± 24.0	0.962 ± 0.005	65 994.0 ± 9.0
0.487 ± 0.016	303 967.0 ± 24.0	0.975 ± 0.005	50 786.0 ± 7.0
0.500 ± 0.016	299 208.0 ± 22.0	0.986 ± 0.005	36 044.0 ± 5.0
0.513 ± 0.015	294 539. ± 22.0	0.992 ± 0.012	24 173 ± 13.0
0.525 ± 0.015	290 349.0 ± 22.0		

the seismic model and are not far from SSM predictions, see Turck-Chièze et al. (2012) and Table 5. This fact shows that the microscopic description of the solar core is quite good and reinforces interest in searching for dark matter.

2.3 The Radial Sound Speed Deduced from *SOHO*

The expression (8) shows that a reference model and a calculation of its mode frequencies are needed to determine the solar sound speed *c(r)* and density $\rho(r)$ profiles. Effectively, these two quantities are obtained from the differences $\delta\nu_{n,\ell}$ between observed and calculated frequencies. We generally use a standard solar model that also allows us to determine the kernels $K_c^{(n,\ell)}(r)$ and $K_\rho^{(n,\ell)}(r)$. This method leads to good results if the model frequencies are not too far from the observed frequencies and if one gets a set of coherent frequencies between them, determined with small error bars. These two conditions are fulfilled in the case of the Sun, except that the absolute values of the observed

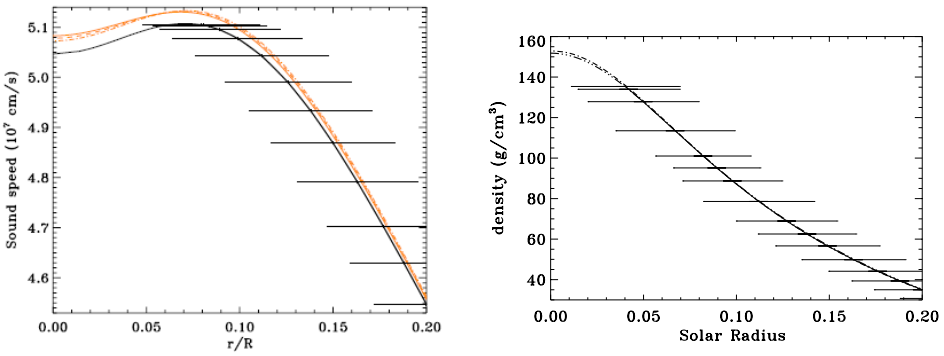

Fig. 5 Enlarged view of the solar core showing the observed sound speed and density profiles obtained with the modes given in Table 1. The corresponding values of the seismic model appears like a continuous line on the sound speed profile and like a dash-dotted line on the density profile. See also Turck-Chièze & Couvidat (2011); Turck-Chièze, Piau & Couvidat (2011b). One also sees the extrapolation done for these two quantities down to the core. Standard model predictions and models with a different energetic balance lead to the sound speed profile appearing in red in the color version of the figure. At these scales, the vertical error bars are so small that they are not visible and all the models seem to be in good agreement, but only the seismic prediction fits all the observed values.

frequencies differ from the theoretical ones for modes that reflect very near the surface; this problem comes from the description of the sub surface layers, see Section 2.5. The way to correct for this is to add in Equation (8), which contains a surface term $Q_{n,\ell}^{-1}G(\omega_{n,\ell})$, in the inversion procedure (Christensen-Dalsgaard 2002)

$$\frac{\delta\nu_{n,\ell}}{\nu_{n,\ell}} = \int_0^R \left[K_c^{(n,\ell)}(r)\frac{\delta c}{c}(r) + K_\rho^{(n,\ell)}(r)\frac{\delta\rho}{\rho}(r)\right] dr + Q_{n,\ell}^{-1}G(\omega_{n,\ell}). \quad (8)$$

The list of low degree acoustic mode frequencies (Table 1), added to the list of higher degree MDI modes (Rhodes et al. 1997), leads to the sound speed given in Table 2, and Figures 5 and 10(a). These profiles correspond to the publications of Turck-Chièze et al. (2001) and Couvidat et al. (2003b). They do not take into account any gravity modes. Equivalent results have been obtained more recently using the BiSON network +MDI. In that last case, the determination of the low degree low order acoustic mode frequencies corresponds to observations with duration of 30 years instead of 4 years for GOLF due to their small amplitude, atmospheric noise and lower duty cycle (Basu et al. 2009). Nevertheless it is a great satisfaction to get firm results from different observations, different models and different inversion methods, all of which reveal a proper determination of the solar observables.

Table 2 also gives the uncertainty of the sound speed determination, which is extremely low (some reach 10^{-4} and even 10^{-5}). Of course it increases at the extremities: few modes are used to describe the center, and the surface turbulence perturbs the frequency of the high degree modes. This absolute uncertainty (not visible in the figure) is largely smaller than the difference between observation and models (see Fig. 10(a)), but the difference with the model predictions does not exceed 1% or 2%. It is useful to know that the radial sound speed varies by only 8%–9% since the beginning of the main sequence due to a compensating effect between the evolution of pressure and composition (see Turck-Chièze, Piau & Couvidat (2011b) for a general discussion of this process).

The radial error bars are also given in Table 2. They result from the kernels of the observed modes. The relatively large error bars in the core are compensated by the accuracy of the obtained

Table 3 Central temperature and density of the seismic model compared to the SSM values (Turck-Chièze, Piau & Couvidat 2011b). The predictions from the boron neutrino flux are compared to the SNO detection: 5.045 ± 0.13 (stat) $\pm$ 0.13 (syst)$\times 10^6$ cm^{-2} s^{-1} (Aharmim et al. 2010). The surface composition of heavy element mass in the SSM model is $Z = 0.0134$ according to the present observation, but the helium surface content is $Y = 0.235$ instead of $Y = 0.25$ deduced from helioseismology.

T_C (10^6 K)	ρ_C (g cm^{-3})	boron ν prediction (10^6 ν cm^{-3} s^{-1})
15.75	153.6	5.31 ± 0.6
15.54	150.6	4.50 ± 0.6

values that strongly constrain the profile (see Fig. 5(a)). The detection of several gravity mode frequencies would probably improve the extraction of the density profile which largely depends on the gravitational potential (Fig. 5(b)). The extraction of the solar internal sound speed has revealed some discrepancy with the classical solar theoretical predictions and has inspired a model that we call the "seismic model." This model has been determined from the structural equations that lead to the Standard Solar Model (SSM) in adjusting the main physical ingredients (opacity, reaction rates) to reproduce the observed sound speed profile. Such a model allows the predictions of neutrinos and gravity modes, and those predictions agree remarkably well with all these observables (Couvidat et al. 2003b; Turck-Chièze et al. 2004b; Turck-Chièze & Couvidat 2011; Turck-Chièze, Piau & Couvidat 2011b).

2.4 The Radial Matter Density Deduced from *SOHO*

Equation (8) shows that the matter density profile is extracted together with the sound speed profile from the comparison of the observed acoustic mode frequencies to model frequencies. Table 4 gives the obtained density profile and Figure 5(b) shows an enlarged view of the solar nuclear core density. Though the radial (horizontal) errors bars remain large in the whole radiative zone, the vertical error bars are so small (not visible in the figure) that they strongly constrain the profile.

The seismic model predictions are in good agreement over the whole radiative zone, see Figure 10(a) and also Turck-Chièze & Couvidat (2011). This extrapolation to the center is particularly useful for the prediction of the gravity modes and for the prediction of the neutrino fluxes (Table 3). In such a model, the nuclear luminosity is required to match the present observed luminosity. As largely discussed in our review on neutrinos, the neutrino predictions of the seismic model agree very well with all the detected neutrinos, taking into account the fact that some electronic neutrinos have been transformed to other types of neutrinos when they arrive at the ground detectors.

The agreement between seismic observations and seismic model results is much better than with the SSM predictions which include the Asplund et al. (2009) photospheric composition (Turck-Chièze, Piau & Couvidat 2011b). This is also true for the neutrino side (see Table 3).

Table 3 shows the central conditions of the models and the predicted boron neutrino flux that is largely temperature dependent ($T^{20} - T^{24}$). Its emission presents a maximum around 5% of the central solar radius. So one may consider the seismic central density and temperature predictions as the most probable values representing the Sun today. This information is crucial in the search for dark matter. In the case of WIMP candidates, one needs to properly describe the very central region. The first detection of gravity modes and the agreement between their prediction and the observed

Table 4 Observed solar density profile obtained by GOLF and MDI instruments located aboard *SOHO*. From Turck-Chièze et al. (2001); Couvidat et al. (2003b).

$r/R_\odot$	Density (g cm^{-3})	$r/R_\odot$	Density (g cm^{-3})
0.040 ± 0.029	135.35 ± 0.06	0.525 ± 0.016	1.0530 ± 0.0004
0.042 ± 0.027	133.98 ± 0.07	0.537 ± 0.015	0.9340 ± 0.0004
0.050 ± 0.03	127.86 ± 0.06	0.550 ± 0.015	0.8218 ±0.0003
0.067 ± 0.032	113.49 ± 0.05	0.562 ± 0.015	0.7311 ± 0.0003
0.082 ± 0.025	101.03 ± 0.04	0.575 ± 0.015	0.6449 ± 0.0003
0.089 ± 0.023	95.14 ± 0.03	0.587 ± 0.014	0.5752 ± 0.0002
0.098 ± 0.027	88.72 ± 0.02	0.600 ± 0.014	0.5088 ± 0.0002
0.112 ± 0.030	78.59 ± 0.02	0.613 ± 0.014	0.4507 ± 0.0002
0.127 ± 0.027	68.93 ± 0.02	0.625 ±0.014	0.4035 ± 0.0002
0.138 ± 0.026	62.53 ± 0.018	0.638 ± 0.013	0.3585 ± 0.00015
0.149 ± 0.028	56.65 ± 0.014	0.650 ± 0.013	0.3218 ± 0.00014
0.163 ± 0.028	49.84 ± 0.012	0.663 ± 0.013	0.2868 ± 0.00012
0.176 ± 0.026	44.14 ± 0.011	0.675 ± 0.013	0.2584 ± 0.0001
0.188 ± 0.026	39.36 ± 0.009	0.688 ± 0.012	0.2315 ± 0.0001
0.200 ± 0.026	34.999 ± 0.008	0.700 ± 0.012	0.20974 ± 9.e–5
0.213 ± 0.025	30.720 ± 0.007	0.713 ± 0.011	0.18928 ± 8.e–5
0.225 ± 0.024	27.164 ± 0.006	0.725 ± 0.011	0.17333 ± 7.5e–5
0.238 ± 0.024	23.717 ± 0.005	0.737 ± 0.011	0.15814 ± 7.e–5
0.250 ± 0.023	20.884 ± 0.004	0.750 ± 0.010	0.14269 ± 6.e–5
0.262 ± 0.023	18.359 ± 0.003	0.763 ± 0.01	0.12823 ± 5.5e–5
0.275 ± 0.022	15.935 ± 0.003	0.775 ± 0.01	0.11575 ± 5.6e–5
0.288 ± 0.022	13.804 ± 0.0025	0.787 ± 0.01	0.10403 ± 4.6e–5
0.300 ± 0.021	12.074 ± 0.002	0.800 ± 0.0094	0.09218 ± 4.0e–5
0.312 ± 0.021	10.554 ± 0.0019	0.812 ± 0.0091	0.08200 ± 3.60e–5
0.325 ± 0.021	9.119 ± 0.0016	0.825 ± 0.009	0.07170 ± 3.1e–5
0.337 ± 0.020	7.967 ± 0.0014	0.837 ± 0.009	0.06290 ± 2.7e–5
0.350 ± 0.020	6.881 ± 0.0013	0.850 ± 0.008	0.05404 ± 2.4e–5
0.363 ± 0.020	5.943 ± 0.0011	0.862 ± 0.008	0.04650 ± 2.0e–5
0.375 ± 0.019	5.195 ± 0.001	0.875 ± 0.008	0.03897 ± 1.7e–5
0.387 ± 0.019	4.546 ± 0.001	0.887 ± 0.008	0.032612 ±1.4e–5
0.400 ± 0.0185	3.9377± 0.0008	0.900 ± 0.0075	0.026329 ± 1.2e–5
0.412 ± 0.018	3.4505 ±0.0008	0.912 ± 0.007	0.0210828 ± 9.4e–6
0.425 ± 0.018	2.9929 ± 0.0007	0.925 ± 0.007	0.0159947 ± 7.2e–6
0.437 ± 0.0176	2.6283 ± 0.0007	0.937 ± 0.007	0.0118365 ± 5.4e–6
0.450 ± 0.017	2.2872 ± 0.0006	0.950 ± 0.008	0.00792621 ± 3.7e–6
0.462 ± 0.017	2.0139 ± 0.0006	0.962 ± 0.008	0.00488241 ± 2.4e–6
0.475 ± 0.017	1.7562 ± 0.0005	0.975 ± 0.010	0.0022403 ± 1.16e–6
0.487 ± 0.016	1.5498 ± 0.0005	0.987 ±0.014	0.0005954 ± 3.5e–7
0.500 ± 0.016	1.3562 ± 0.0005	0.990 ± 0.060	0.000327 ± 3.e–7
0.512 ± 0.016	1.2006 ± 0.0004		

values (see Tables 1 and 5) also show that the solar core representation is reasonably well controlled, even though one would be happy to improve the detection of these modes (see Sect. 4).

2.5 Subsurface Layers, Manifestations and Origins of Cycles

We have shown that the seismic solar model is a good guide to get an internal physical description of the solar radiative zone. But we have also mentioned that the observed acoustic mode frequencies vary and differ from the theoretical ones at high frequencies.

Table 5 gives some predicted values that illustrate this fact and Figure 6 shows the comparison for all the acoustic modes detected by GOLF. One sees, comparing Table 5 to Table 1, or looking to Figure 6, that below 2400 μHz, the theoretical values generally agree with the observed frequencies

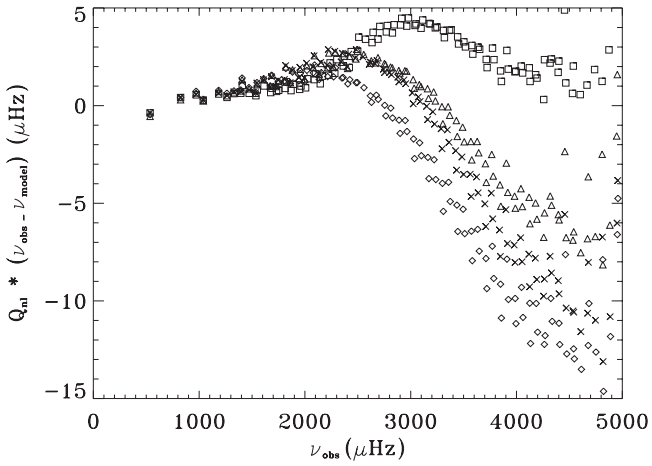

Fig. 6 Normalized difference between observed GOLF frequencies and theoretical frequencies of the SSM using MLT convection (*diamonds*), the Canuto description of convection (*triangles*) (Canuto & Mazzitelli 1991), mean thermal description (*crosses*) and 3D simulation of Nordlund & Stein (2000) (*squares*). From Piau et al. (2012).

Table 5 Some seismic model frequencies from Turck-Chièze et al. (2004a); Mathur et al. (2007)

$\ell = 1$, $n = -10$: 62.5 μHz	$\ell = 1$, $n = -4$: 127.4 μHz	$\ell = 2$, $n = -3$: 222.1 μHz	$\ell = 1$, $n = 1$: 257.7 μHz
$\ell = 0$, $n = 10$: 1548.9 μHz	$\ell = 0$, $n = 16$: 2364.4μHz	$\ell = 0$, $n = 25$: 3585.7 μHz	$\ell = 0$, $n = 35$: 4964.3 μHz

within about 1 μHz (slightly more for the standard model) and that the difference increases with frequency.

Above 2400 μHz, the frequencies vary cyclically with the 11 year cycle of 0.5 μHz at maximum and a second smaller periodicity in amplitude of about 2 years is clearly visible in all the data at all frequencies (Fletcher et al. 2010; Simoniello et al. 2012). The difference between predictions and observations is mainly due to a poor description of the last 2% of the solar radius ($-14\,000$ km from the surface) and the variabilities could also come from this region.

Indeed, that region, just below the surface, has very rich physics: at about –1.5% (about $-10\,000$ km) the partial ionization of helium produces a strong change in the adiabatic exponent and consequently in the opacity, then at -0.5% (-3500 km) there is an equivalent effect for hydrogen, see figure 1 of Lefebvre et al. (2009) and the consequences of a variation of radius. Above, the superadiabatic region begins, the opacity decreases suddenly due to the formation of molecules, and both radiation and convection transport the energy toward the surface, then at –0.02% (–150 km) there appears a turbulent peak in the 1D model. Rosenthal et al. (1999) have shown that 3D modeling of the convection in this region is useful to better describe this turbulence. Indeed this phenomenon is not so sharp in the simulation and influences the gas pressure down to –5000 km, practically the first 1% below the surface. In coupling the 1D model to the 3D model, using the STAGGER code, Nordlund & Stein (2000); Piau et al. (2012) have shown that convection is chiefly responsible for the differences in frequency between theoretical predictions and GOLF observations, at high frequency (see Fig. 6). In 1D, the prescription of Canuto & Mazzitelli (1991) already gives better results than the mixing length theory (MLT), but the 3D simulation reduces the differences between observations

and predictions to within 5 μHz. There is indeed another contribution of about 3 μHz that comes from non adiabatic effects.

Regarding variability, if it is generally believed that the origin of the 11 year cycle is located at the level of the tachocline (transition between solid rotation to differential rotation at the base of the convective zone, see Sect. 4), the manifestation of the 11 year variability in the acoustic mode frequencies (visible above 2400 μHz, Fig. 3(a) helps to visualize the cavities corresponding to the different frequencies) is located just below the surface (–0.1% or –700 km). In fact, at this depth, the magnetic pressure is no longer negligible compared to the gas pressure. For the biennial variability, a second dynamo is discussed but as there is no latitudinal dependence and no variability with frequency, one cannot exclude that this biennial effect is due to some kappa mechanism in the layers where helium or hydrogen opacities vary as the sub surface layers slightly move with time because of activity (Lefebvre et al. 2009). If this is the case, the origin of this perturbation could be located in the region 1%–2% below the surface.

These variations in subsurface structure related to the solar magnetic cycle also cause variations of the total solar luminosity on the order of 0.1%–0.2%. By reconstructing the total luminosity variation during the last 7000 years from the ^{14}C variations produced by cosmic-ray fluctua-tions induced by the 11 year solar cycle, it was possible to show that such variations in luminosity are quite common in the Sun (Passos et al. 2007). Furthermore, during the last 500 years, the Sun shows a clear trend of magnetic activity, well above the average of the previous 6500 years. Its present luminosity is larger than the average luminosity for the period.

At the end of this section, one can say that the *SOHO* satellite, accompanied by networks and neutrino detections, has impressively revealed the solar radiative zone and has shown magnetic variabilities only coming from the subsurface region. These observations are nicely reproduced by more sophisticated models than the standard one (see also Sect. 4). The core of the Sun is better understood today than any other stellar core, so it places the Sun at a privileged position for looking for constraints on dark matter, as was suggested 25 years ago by Spergel & Press (1985). At that time, the motivation was to clarify the neutrino puzzle (Cox et al. 1990; Giraud-Heraud et al. 1990; Dearborn et al. 1991; Kaplan et al. 1991); today the main objectives are to contribute to determining some properties of dark matter and motivate new efforts at detection.

3 DARK MATTER

Dark matter is a fundamental ingredient in the evolution of the Universe. Its presence appears in a multitude of cosmological observations and numerical simulations (Teyssier 2002; Springel et al. 2005; Teyssier et al. 2009), and is today firmly established within the framework of the standard model of cosmology (e.g. Komatsu et al. 2011). In terms of energy contents, our Universe is constituted by about 4% *baryonic matter*, 23% *dark matter* and 73% *dark energy*. The presence of an adding gravitational force attributed to dark matter has been identified in the velocity of galaxies in clusters, the rotation curves of galaxies, the cosmic microwave background anisotropies, the velocity dispersion of dwarf spheroidal galaxies and is most likely at the origin of observed gravitational lensing (Frieman et al. 2008). These facts suggest that the constitutive particles of dark matter responsible for this extra gravitational field are probably massive, non-baryonic and non-relativistic, and also interact weakly with regular baryonic matter (Bertone et al. 2005).

Particle physicists have proposed several dark matter candidates based upon an extension to the standard model of particle physics where the particles are classified in three groups: symmetric particles, asymmetric particles and exotic particles (Feng 2010). In the framework of observational and theoretical cosmology, particles that include most of the critical properties are referred to as WIMPs. They interact gravitationally with other particles and scatter with baryons on the weak scale. WIMPs are among the most popular cosmological type of dark matter candidates. Such class of particles occurs in several symmetric extensions of the standard model of particles, like the super-symmetric

(SUSY) model (Jungman et al. 1996). In such a model, the ideal WIMP is the neutralino, which is a stable particle, the lightest super-symmetric particle, and a Majorana particle with a self-annihilation cross section of the order of the weak-scale interaction. It can also be an asymmetric particle which also has interactions with baryons at the weak-scale but does not self-annihilate (Kaplan et al. 2009). Unlike symmetric particles, these particles carry a conserved charge analogous to the baryon number asymmetry. As a consequence of dark matter being asymmetric, there is an unbalanced amount of particles and antiparticles, introducing an asymmetric parameter in the dark matter identical to the so-called baryonic asymmetry. These asymmetric models suggest that the fundamental asymmetric particle has a mass of at least a few GeV (Cohen et al. 2010; Kang et al. 2011).

3.1 Direct Dark Matter Search

The firm establishment of dark matter prompted the development of detectors built to demonstrate the existence of dark matter by a direct detection of the scattering of dark matter particles with baryons, or by finding a by-product resulting from the annihilation of dark matter particles. Dark matter particles interact through two types of scattering cross sections: spin-independent (SI) cross section or spin-dependent (SD) cross section. In general, the scattering cross section is proportional to the reduced mass of the system of colliding particles. In the case of heavy elements, the coherent scattering cross section becomes proportional to the square of the atomic number of the target nucleus. The spin-dependent scattering cross section is the dominant term for the collision of dark matter particles with hydrogen and the spin-independent scattering cross section is the dominant term for the heavier elements (Lopes et al. 2011). The indirect dark matter search is determined by observational constraints obtained from the by-products of dark matter annihilation such as gamma rays or high-energy neutrinos, which are estimated from the expected annihilation rates of dark matter which is gravitationally trapped inside large gravitational fields, such as the galaxy's center, the center of the Sun or the center of the Earth (e.g., Bertone et al. 2005).

The principle of detection consists of measuring the energy deposited by the dark matter particle or by its by-product. This approach is based on the fact that dark matter particles or their by-products, located in a dark matter halo, go through the detectors like through our Earth or the Sun. Most of the related experiments have obtained upper bounds on the scattering cross section of nuclei as a function of the mass of the dark matter particle (Hooper & Baltz 2008). Nevertheless, each experiment depends on the specific parameters of dark matter candidates that were being considered, namely, the mass of the particle, the spin-dependent and spin-independent scattering cross section and the annihilation cross section. Several upper bounds have been determined. In the case of the spin-dependent scattering cross section, the upper limit is $10^{-38}\ \mathrm{cm}^2$ (Archambault et al. 2009).

In the case of the spin-independent scattering cross section, most of the direct detection experiments found null detection within the range of parameters for which the experiment was sensitive, such as the XENON10/100 collaboration (Xenon100 Collaboration et al. 2012), the CDMS collaboration (Ahmed et al. 2011) and the SIMPLE collaboration (Felizardo et al. 2012). Current experimental upper exclusion limits are fixed for light dark matter (≤ 16 GeV) to be of the order of $10^{-39} - 10^{-42}\ \mathrm{cm}^2$ (e.g., Lopes & Silk 2012). Nevertheless, there are a few other experiments that are in contradiction with the previously mentioned ones and which claim to have found evidence of a positive detection. These are the DAMA/LIBRA and CoGeNT experiments (Bernabei et al. 2008; Aalseth et al. 2011). These experiments detect the presence of dark matter using a different physical principle, which takes into account the motion of the Earth around the Sun (Drukier et al. 1986). This result is also corroborated by the CRESST experiment (Brown et al. 2012) which also found some unexplained events.

The interaction of the dark matter particle with baryons is usually considered within the framework of classical interaction between particles, but one cannot exclude the case that the interaction could be slightly different. Several authors (Hooper & Kelso 2011; Farina et al. 2011; Del Nobile

et al. 2011) have proposed theoretical solutions that accommodate current positive detection experiments with previous null ones, such as inelastic scattering (endothermic or exothermic reaction), velocity suppressed interactions, momentum dependent scattering and resonant scattering. Among them, one of the more appealing theoretical explanations is to consider that a dark matter particle couples unequally to protons and neutrons of the colliding nuclei (Kurylov & Kamionkowski 2004; Giuliani 2005), a physical process usually referred to as isospin violation.

3.2 Dark Matter Interaction Inside Stars

The formation of primordial stars occurred within a halo of dark matter, a very common structure at the beginning of the Universe. The most common substructures were small, compact dark matter halos, usually referred to as mini-halos, and were the site of a strong gravitational field that attracts a large amount of baryons. The constant accretion led to the formation of the first clouds of baryons. Some of these mini-halos became the birthplace of the first generation of stars (Ricotti & Gould 2009). These mini-halos later assimilated into larger dark matter structures, producing the first galaxies. In the current Universe these dark matter halos became farther apart and less dense. Nevertheless, it is believed that each spiral galaxy is immersed in a dark matter halo.

The dark matter density in the solar neighborhood was estimated to be of the order of $0.2 - 0.8\ \mathrm{GeV\ cm^{-3}}$ from the motion of stars and molecular clouds in the Milky Way (Turner 1986; Bertone et al. 2005). Presently the most reliable estimation (Catena & Ullio 2010) gives a local density of dark matter $\rho_{\mathrm{DM}} \sim 0.385 \pm 0.026\ \mathrm{GeV\ cm^{-3}}$. The dark matter in the solar neighborhood is supposed to be constituted by particles in thermal equilibrium with a Maxwellian velocity dispersion of the order of $270\ \mathrm{km\ s^{-1}}$ (Jungman et al. 1996).

Nevertheless, in other regions of the local Universe, the dark matter density is much higher, like in the nucleus of galaxies, including that in the Milky Way. The dwarf spheroidal galaxies in the Milky Way's neighborhood have large mass-to-light ratio values which suggest that these galaxies have a very large amount of dark matter, namely in the central regions (Irwin & Hatzidimitriou 1995). In some cases, the density is expected to be ten million times the dark matter density in the solar neighborhood. In recent years, several ultra faint spheroidal dwarf galaxies have been found in the halo of the Milky Way that exhibit extremely low stellar densities (Willman et al. 2005). Some of them present a very large mass-to-light ratio, implying them to be completely dominated by dark matter (Casas et al. 2012). While the dwarf spheroidal galaxies have mass-to-light ratios up to 100, the ultra faint spheroidal dwarf galaxies have mass-to-light-ratios of up to $\sim$1800, assuming the satellites are in virial equilibrium.

For stars evolving within such a dark matter environment, most dark matter particles will continue on their paths through the stellar interior unperturbed. However, occasionally a few of them will scatter off a baryon-nuclei losing part of their kinetic energy. Depending on the specific properties of the dark matter particles, this loss of energy results in the fact that the dark matter particle is trapped in the stellar interior. The particle is no longer able to escape the stellar gravitational field, because the velocity of the dark matter particle is smaller than the escape velocity of the star. Consequently, the more massive stars that have a larger escape velocity capture a larger amount of dark matter. A dark matter halo located in the solar neighborhood has formed by dark matter particles with a mass 10 GeV; the total mass of dark matter accumulated during the evolution of a low mass star like the Sun is smaller than $10^{-12}\ M_{\odot}$. The contribution of dark matter to the total mass of the star is totally negligible, but the presence of dark matter in the stellar interior changes the local properties of the plasma, and by doing so will affect the evolution of the star. In general, the evolution of a star within a dark matter halo is very similar to the evolution of a regular star, but the presence of dark matter causes a few important differences that can produce visible effects in the structure and evolution of the star (Scott et al. 2009; Taoso et al. 2010; Lopes et al. 2011).

3.3 Implementation of WIMP Interactions in Stellar Codes and the Solar Signature

The impact of dark matter on the evolution of a star happens through two basic mechanisms: the modification of the energy transport within the different regions of the star, and the creation of an extra source of energy resulting from the annihilation of dark matter particles. The former mechanism is more important for stars in a low density dark matter halo, like in the solar neighborhood. This is the case in a star like the Sun (Giraud-Heraud et al. 1990; Dearborn et al. 1991). The latter mechanism is more pronounced in a high density dark matter halo, with several million times the dark matter density of the solar neighborhood (Salati & Silk 1989). This type of scenario occurs in stellar populations located in the center of galaxies, including the Milk Way, in certain stellar populations of spheroidal galaxies, or during the formation of the first generation of stars in the primordial Universe. In both cases, these effects are more pronounced in the case of stars with low mass, for which dark matter enhances the transport of energy and increases its production inside the star in a way that distinctively affects the evolution of the star.

The amount of dark matter present in the stellar core is mainly regulated by the capture rate of dark matter. Capture rates of dark matter were first calculated by Press & Spergel (1985) in the case of the Sun, by Gould (1987) for generic massive bodies, and by Bouquet & Salati (1989) for main sequence stars. Presently, in the most up-to-date codes, the capture rate is computed numerically from the integral expression of Gould (1987) implemented as indicated in Gondolo et al. (2004). The capture rate is proportional to the local dark matter density and the scattering cross section of baryon-nuclei and is inversely proportional to the mass and the dispersion velocity of the dark matter particle (Gould 1987). The equations are the following (see the review papers of Jungman et al. 1996; Bertone et al. 2005; Taoso et al. 2010 for details)

$$\frac{dN_X}{dt} = C - 2AN_X^2 - EN_X, \tag{9}$$

where N_X is the number of WIMPs, C the capture rate, A the annihilation rate and E the evaporation rate. The latter one is generally considered to be negligible for a WIMP mass greater than 5 GeV.

$$C = \sum_i 4\pi \int_0^R r^2 \frac{dC_i(r)}{dV} dr \quad \text{with} \quad \frac{dC_i(r)}{dV} \propto \frac{\rho_i(r)}{M_i} \frac{\rho_X}{M_X} \frac{v^2}{\bar{v}^2} \bar{v} \sigma_{X,N_i}, \tag{10}$$

where $\bar{v}$ is about 270 $\mathrm{km\ s^{-1}}$ and v is about 220 $\mathrm{km\ s^{-1}}$.

$$A = \int_0^R \epsilon_{\mathrm{ann}} r^2 4\pi \rho(r) dr. \tag{11}$$

If one considers an equilibrium between capture and annihilation, $A = C/2$. This hypothesis is often taken inside the Sun at the present age. The total scattering cross section of dark matter with baryon-nuclei σ_{X,N_i} is regulated by two leading parameters: the spin-dependent scattering cross section that is relevant for hydrogen, and the spin-independent scattering cross section that defines the interaction of the dark matter particles with the heavy nuclei.

In a star from population II, like the Sun, we can calculate the capture of dark matter by the following isotope elements: H, ^{4}He, ^{12}C, ^{14}N, ^{16}O, ^{2}H, ^{3}He, ^{7}Li, ^{7}Be, ^{13}C, ^{15}N, ^{17}O and ^{9}Be. The spin-dependent scattering depends mainly on H, and in the case of the spin-independent scattering, the interaction with ^{4}He, ^{14}N and ^{16}O dominates. In final phases of stellar evolution ^{56}Fe, ^{20}Ne and ^{16}O can also capture significant amounts of dark matter (Lopes et al. 2011). The stellar codes explicitly follow the capture rate of the dark matter particles by the different chemical elements present inside the star, with some of them changing in isotopic abundance during the star's evolution. Both scattering processes occur simultaneously, nevertheless, if the value of the spin-independent scattering cross section is larger than a hundredth of the spin-dependent scattering cross section,

then the capture of dark matter particles is dominated by collisions with heavy nuclei, rather than by collisions with hydrogen (Lopes et al. 2011).

The capture of dark matter by a star is a complex process regulated by several physical mechanisms that must be understood and their uncertainties known, in order to permit a proper determination of the amount of dark matter being captured by the star. Among other parameters, it will be important to precisely determine the following ones: stellar parameters, characteristics of the dark matter halo, properties of the dark matter particles, namely, the dark matter annihilation channels and the interaction of dark matter particles with baryons. In Lopes et al. (2011) a detailed discussion of the impact of such uncertainties on the capture rate of dark matter by the Sun and other low-mass stars in different phases of the stellar evolution is presented.

The impact of dark matter on the evolution of a star is more visible in low-mass stars, for which the changes in energy transport caused by the local presence of dark matter particles can compete with the local transport of energy by photons. In dark matter halos of low density, the presence of dark matter inside the star changes the transport of energy, by facilitating the transfer of radiation towards the surface of the star. The left panel of Figure 7 shows a significant temperature change in the core of the Sun due to the presence of WIMPs (Lopes & Silk 2010b) and the right panel of Figure 7, from Lopes & Silk (2010a), shows the impact of dark matter on the different neutrino fluxes for a couple of cross sections mentioned in the figure caption and a specific dark matter mass that leads to a reduction of the central temperature by 4%. Moreover, the calculations of the effect of dark matter are now estimated not only on protons and heavy elements but on all the species that could be detected by neutrino detectors in the coming years (Taoso et al. 2010; Lopes et al. 2011). In dark matter halos with high density, the dark matter annihilation produces an extra source of energy that changes the H-R evolution path of the star (Casanellas & Lopes 2011a). Such physical processes become less significant in the case of more massive stars.

At the end of the eighties, the density of dark matter in the solar neighbor was reasonably estimated to be 0.4 GeV cm^{-3}. The axial and vectorial cross sections were taken to be of the order of pbarns (10^{-36} cm^2). Since WIMPs act like a conductor, they thermalize the core and reduce the central temperature. As a consequence, the predicted boron neutrino flux is reduced. A factor of 2.5–3 was necessary to interpret the chlorine neutrino results by the presence of WIMPs, which corresponds to a reduction of the central temperature by about 10%–15%. At that time, we had shown that if a solution was found for a large domain of mass, the obtained result was contradicted by the sound speed profile (Kaplan et al. 1991), even though this profile was not so well determined at that time. Of course we know now that this neutrino flux reduction was due to the fact that about 66% of the electronic neutrinos are transformed into another flavor of neutrinos before reaching the Superkamiokande detector.

The renewal of interest to look to the impact of dark matter in the Sun today comes from our improved knowledge about the solar core and the hope to put tight constraints on these particles. Four different kinds of detectors have produced a more coherent picture of the neutrino fluxes and they all agree with the seismic neutrino flux predictions that include the change of neutrino flavors (Turck-Chièze & Couvidat 2011). So the uncertainty in the central temperature is largely reduced ($< 0.5\%$). The detection of acoustic modes and the development of the seismic model have shown (see Sect. 2.3 and Tables 2, 3, and 5) that all the observations, both acoustic modes and boron neutrino fluxes, privilege a slight increase of the central temperature and a slight decrease of the density in comparison with the SSM predictions. This effect is opposite with regard to a signature of WIMPs, so it can help to put limits on the properties of these particles (Turck-Chièze et al. 2012).

To be complete or at least coherent between observations, one also needs to check the density profile in the solar core. This information is largely determined by the gravity mode properties (see Eqs. (6) and (7)) for which we verified the coherence with seismic model predictions.

Figure 8(a) illustrates the impact of the dark matter interaction for masses of dark matter between 3 and 12 GeV, relatively high spin dependent cross section and self annihilating particles (Lopes &

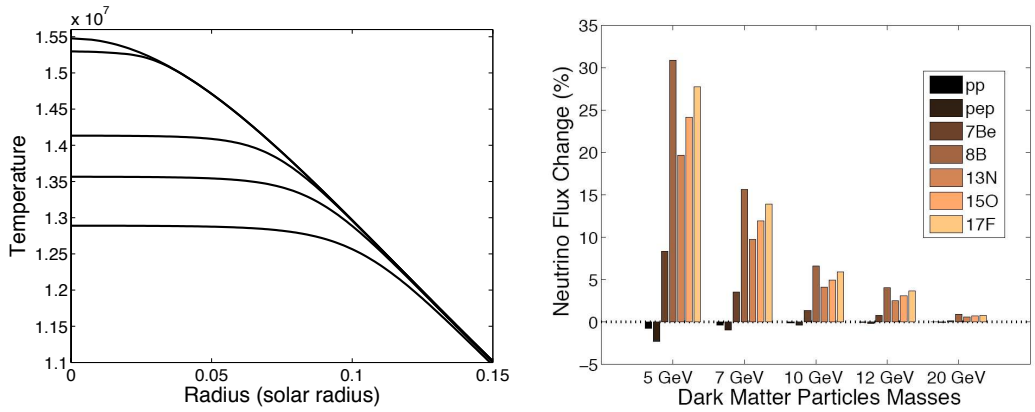

Fig. 7 *Left*: Comparison of temperature profiles between SSM and models of the Sun evolving in different dark matter halos of non-annihilating particles: 5 GeV, 7 GeV, 10 GeV and 50 GeV (from low to higher temperature). In these models, particles interact with baryons with a spin-dependent scattering cross section of the order of 2×10^{-35} cm^2, and spin-independent scattering cross sections of the order of 10^{-40} cm^2 (no effect). The black curve with the highest central temperature corresponds to the SSM (Lopes & Silk 2010b). *Right*: Comparison of the predicted neutrino fluxes, between SSM and models of the Sun evolving in halos of dark matter where dependent and independent scattering cross sections with baryons are respectively 2.0×10^{-35} cm^2 and 4.0×10^{-40} cm^2. The product of the self annihilation cross section and the relative velocity of colliding particles at freeze-out is of the order of 1.0×10^{-36} cm^{3}s^{-1} (Lopes & Silk 2010a).

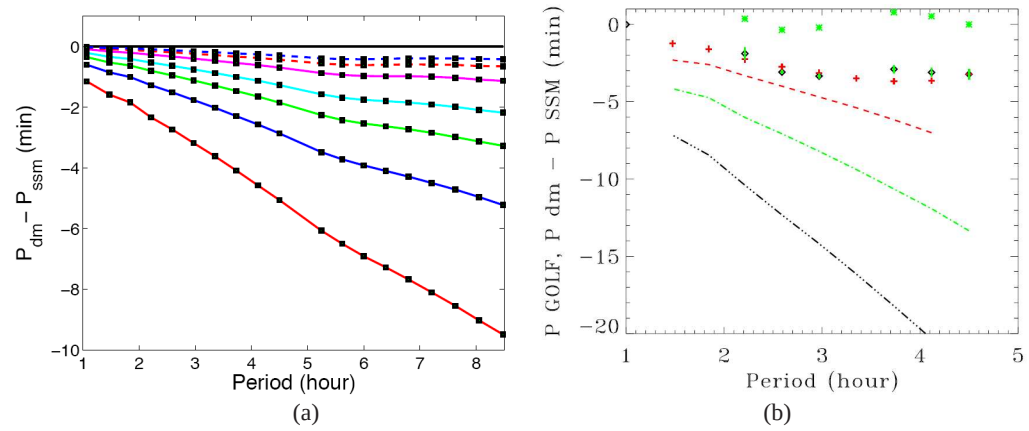

Fig. 8 (a) Comparison of the predicted periods $P_{n,\ell}$ of the dipole gravity modes $\ell = 1$, between SSM and models of the Sun evolving in a dark matter halo with annihilating massive particles from 3 to 12 GeV. From Lopes & Silk (2010b). (b) Idem between GOLF and SSM (*circles with error bar*), GOLF and seismic and SSM models or (*crosses*), GOLF and SSeM (*stars*). Superimposed are DM non annihilation models with a spin dependent cross section of 5×10^{-36}cm^2 for respectively 5, 7 and 10 GeV (black, green and red line). From Turck-Chièze et al. (2012).

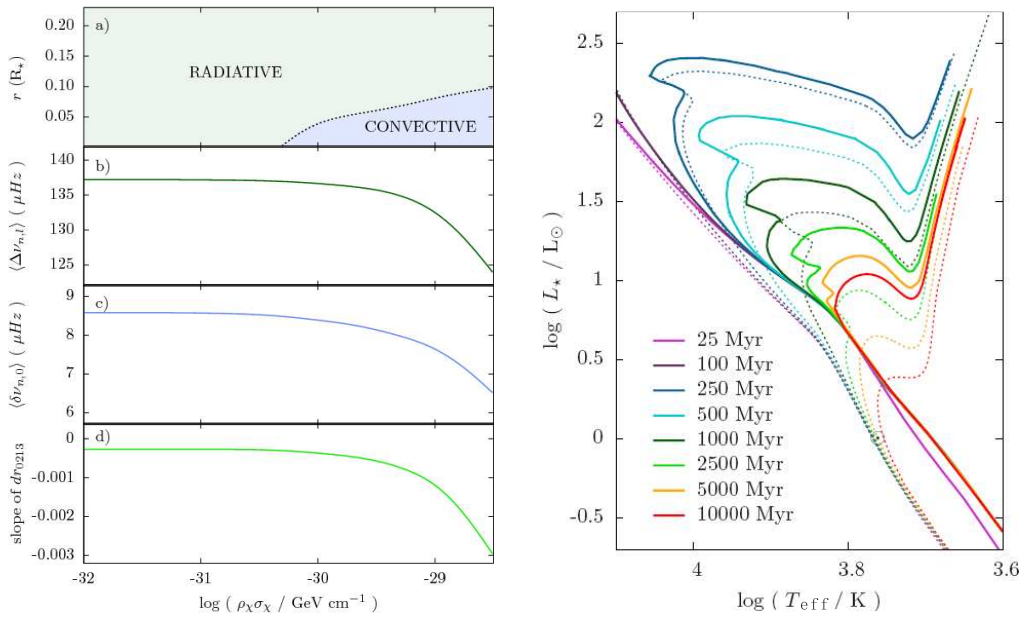

Fig. 9 *Left*: (a) Size of the convective core, and the calculated seismic parameters: (b) mean large separation (for $l = 0, 1, 2, 3$), (c) mean small separation (for $\ell = 0$) and (d) slope of dr_{0213}, for 1 $M_\odot$ stars that evolved in DM halos with different densities ρ_χ and SD WIMP-nucleon cross sections $\sigma_{\chi,\mathrm{SD}}$, when the stars reached a luminosity $L = 1\ L_\odot$. See Casanellas & Lopes (2011b) for the definitions of the seismic parameters. Right: Isochrones for a cluster of stars with masses between 0.7 $M_\odot - 3.5\ M_\odot$ that evolved in a halo of DM with a density $\rho_\chi = 10^{10}$ GeV cm^{-3} (*continuous lines*) and for the same cluster in the classical scenario without DM (*dashed lines*). See Casanellas & Lopes (2011a) for the details.

Silk 2010b) in comparison with the SSM model of Turck-Chièze & Lopes (1993). The effect clearly increases with the period (or with the order n) of the modes and decreases with the dark matter mass. This effect largely decreased when spin dependent cross section decreases. A detailed analysis has been done using both gravity modes and neutrinos in the domain of dark matter cross sections that are not rejected by previous analyses. No detectable signature of the annihilation cross section has been seen. For a spin dependent cross section of 5×10^{-36} cm^2 and a spin independent cross section of 10^{-40} cm^2.

Figure 8(b) compares the period of the dipole gravity modes for models including dark matter in the range of mass between 5 to 10 GeV to predictions of the SSM model, measured gravity modes and predictions of the seismic model. This detailed comparison, done also for other couples of cross sections, does not favor any effect of dark matter. The confrontation of all the results disfavor the presence of non-annihilating WIMPs for masses smaller than 10–12 GeV and spin dependent cross sections greater than 5.0×10^{-36} cm^2 (Turck-Chièze et al. 2012). In fact, an analysis of the boron and beryllium neutrino results alone confirms these results for a spin independent cross section greater than 3.0×10^{-37} cm^2 (Lopes & Silk 2012). Such range of exclusion does not contradict other works, but could be in contradiction with the claim of possible detection of these particles.

Such analysis will be pursued in the future with all the different species of neutrinos and with an extended range of detection of gravity modes in a future space mission (see Sect. 4).

3.4 Dark Matter and Other Stars, Asteroseismology and Stellar Clusters

The Sun is efficient in limiting the properties of dark matter candidates and the detection of both gravity modes and neutrinos will continue to deliver more and more constraints. But our Sun is located in a dark matter halo region of very low density. The diagnosis of certain dark matter candidates can strongly improve if we choose to study the impact of dark matter in other regions of the Universe, where the dark matter density is much higher than in the solar neighborhood. A typical example is the evolution of stars in the center of galaxies. In looking toward the galaxy's center, Iocco et al. (2012) show that a signature must be visible for solar mass stars placed in DM densities of $\rho_X \geq 102\,\mathrm{GeV\ cm^{-3}}$. In these cases, their central region shows differences down to a spin-dependent scattering cross section $\sigma_{\mathrm{SD}} \geq 10^{-37}\ \mathrm{cm}^2$ and a DM particle mass as low as 5 GeV.

Another possibility is to study the effect on stars of different masses, different chemical compositions and other phases of evolution that can probe a different set of dark matter particle parameters. Two independent diagnostic tools are quite adequate for such type of studies: the study of stellar cluster populations and asteroseismology. This diagnostic can be used in cases where dark matter contributes to the transport of energy inside the star, or in the case of high density halos for which the annihilation of dark matter particles produces an extra source of energy in the core of the star. This is the case for stellar populations located in the galactic center or in dwarf spheroidal galaxies. In some low-mass stars, the dark matter produces important changes to the local plasma leading to the creation of a convective core which otherwise would be a radiative one (Scott et al. 2009). This type of dark matter signature can be detected by means of asteroseismology (see Fig. 9). The dark matter can also be probed in stellar populations located in regions with high dark matter density. In effect, the evolution track of the star in a dark matter halo could in certain cases follow quite distinct paths from a classical star, due to the energy produced by dark matter in the stellar core. This extra source of energy significantly prolongs the evolution of the star in each stellar phase, makes important changes to the global properties of the star, and consequently also causes changes to the Hertzsprung-Russell path for these stellar clusters (Casanellas & Lopes 2009, 2011a). The presence of dark matter changes, in a very visible way, the main sequence of stellar clusters, as shown in Figure 9 right. Similar physical processes occur in the first generation of stars which have been strongly influenced by the presence of dark matter (Scott et al. 2011; Ilie et al. 2012). The study of stellar clusters in high density dark matter halos has the potential to put important constraints on dark matter properties.

The study of the impact of dark matter on the evolution of stars in the local and primitive Universe appears to be a very promising research field with diversity of applications of interest for the study of dark matter and their implications for astrophysics, cosmology and particle physics.

4 OPEN QUESTIONS

4.1 Radiative Transfer, Energetics, Sterile Neutrino and Dark Matter

The previous section has shown the effect of WIMP dark matter candidates on the central region of stars; in the present one, we extend our analysis to the whole radiative zone of solar-like stars.

Figure 10 shows the *SOHO* results, in terms of squared sound speed, density and rotation profiles for the whole internal Sun. Figure 10(a) shows the differences between observations given in Tables 2 and 4 and SSM or seismic model predictions. At the scale of the figure, the error bars, superimposed on the seismic model, are not clearly visible but are much smaller than the differences between observations and SSM predictions, as mentioned previously. These differences clearly appear in the radiative zone and at the surface. The effect at the surface is now reasonably well understood and discussed in Section 2.5. Here we concentrate on the radiative zone.

Up to now, the differences in the radiative zone have not received a clear explanation. They have been substantially increased by the introduction of the recently measured CNO photospheric

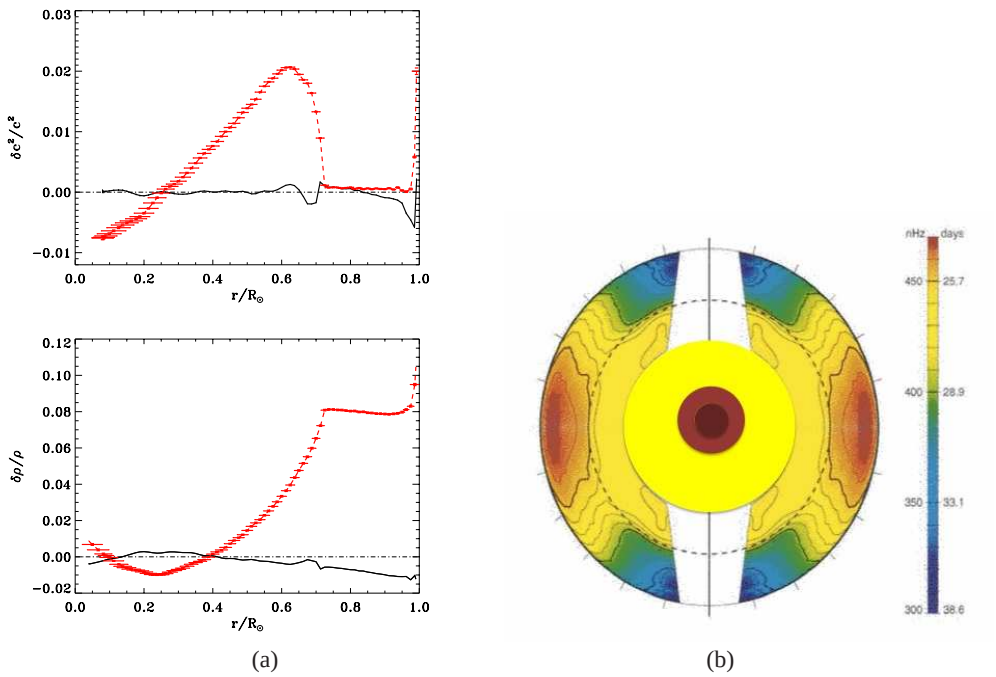

(a) (b)

Fig. 10 (a) Differences in squared sound speed $(c^2_{obs} - c^2_{mod})/c^2_{mod}$ and density $(\rho_{obs} - \rho_{mod})/\rho_{mod}$ profiles between GOLF+MDI/*SOHO* and solar model predictions. Seismic model: full line + seismic error bars, SSM model (−−) using the most recent updated physics. These differences take into account the most recent photospheric composition of Asplund et al. (2009). See Turck-Chièze & Couvidat (2011). (b) 2D representation of the internal rotation extracted from *SOHO* (GOLF+MDI) acoustic modes and the gravity modes seen by the GOLF instrument.

abundance. This fact is easily seen if one compares Figure 10(a) to the figures given in Couvidat et al. (2003b) using the same data but published before this composition update. Some doubt was raised on the quality of the CNO determination (Bahcall et al. 2005) or on the knowledge of neon which is not observed in the photosphere, but the reduction of the photospheric CNO abundance has been confirmed by different groups and definitively established by Asplund et al. (2009). This revision, announced by Turck-Chièze et al. (1993), suppresses the oxygen anomaly of the Sun in comparison with its neighbor and leads to a strong deviation of the observed sound speed compared with the SSM one (see figs. 1 and 2 of Turck-Chièze et al. 2004b).

So, today the hypotheses of the SSM or some of its inputs are under suspicion, in particular the opacity coefficients of this model. It is a purely theoretical model with minimal structural equations, and including no effect of radial differential rotation, meridional circulation or magnetic field. The seismic model is useful today because it uses the same equations but is built to reproduce the seismic acoustic information by only modifying some inputs. It allows predictions of the other observables and supports evidence of the coherence between them. It is not built to better understand the physics, but it contributes to estimating the sensitivity of reactions: only a 1% change in the pp reaction rate has been introduced in that model, and to opacities that need to be changed by 3%–5%. A recent work also shows that the discrepancies are not explained by the transport of momentum by rotation during the main sequence, in fact, such an effect even slightly increases the differences (Turck-Chièze et al. 2010).

The solar radiative transfer is naturally in question because the sound speed is related to the thermodynamical equations by the following relations

$$c^2(r) = \frac{\gamma_1(r)P(r)}{\rho(r)} \propto \frac{T(r)}{\mu(r)}, \tag{12}$$

where γ_1 is the adiabatic exponent, and P, ρ, T, and μ are respectively the pressure, density, temperature and mean molecular weight at each mesh point r. Different aspects of this problem are under study. The first question is the reliability of the opacity calculations at the level that we are looking for. A 30% change in CNO composition has an impact of about 3%–5% on the mean Rosseland opacity in the radiative zone mainly below the base of the convective zone, moreover the recent composition enhances the role of iron in comparison to oxygen; iron is the only element partially ionized in the whole radiative zone (Turck-Chièze et al. 1997, 2009a). The accuracy of such opacity calculations is about 5%, but elemental spectral calculations can show larger variations that will directly impact microscopic diffusion. It is why some comparison between opacity calculations are under study and we hope for some progress in the coming years that cannot exclude some consequent slight composition difference between the radiative zone and the photosphere (Turck-Chièze et al. 2011b).

Another way to look to the same problem is to compare the central temperature of the Sun in the seismic model and in the SSM, and translate the difference in terms of extra lost energy. One can interpret the result as a missing energy of about 5%–6%, which could be attributed to other contributors absent in the structural equations (Turck-Chièze, Piau & Couvidat 2011b). It could be due to the presence of kinetic energy, meridional circulation or magnetic energy that has been lost in the radiative zone during the last million years or it can be due to another transfer of energy.

It is in that scheme that one can introduce the second candidate of dark matter, the sterile neutrino. This particle in the keV range is not yet observed but a renewed interest in this particle appeared over the last few years in the interpretation of the reactor antineutrino flux anomaly (Mention et al. 2011). It is interesting to notice that the impact of the existence of such a particle on the ^{7}Be neutrino flux or on the calibration of the GALLEX solar neutrino experiment was estimated to be only a few percent, which is largely inside the present uncertainties of predictions compared to detections. Such an uncertainty might be reduced in the future. Secondly, the sterile neutrino seems to be a reasonable candidate for warm dark matter with some advantages over cold dark matter (de Vega & Sanchez 2010). Of course due its potential mass, the effect of a such particle on the energy transfer will have neither a specific location in the Sun nor a specific signature, and it will be very difficult to separate this process from any other previously mentioned ones.

Another way to take into account dark matter in stars, without trying to consider a specific particle, is to introduce the component of dark matter as a second source of gravitational potential, as is generally done in most of the simulations of dark matter for the formation of structures in the Universe or in the analytical approach to properly take into account gas and dark matter dynamics (Chieze et al. 1997). As far as we know, this approach has never been used in stellar evolution and it would certainly be interesting to also consider such an approach.

4.2 The Time Evolution of the Rotation Profile, the Young Sun and the Present Sun

In previous sections, we have mainly discussed the internal static Sun and solar-like stars. A step further is to put new constraints on the dynamics of the solar interior. A lot of works have been dedicated to the convective zone and the dynamo of the eleven year cycle. Here we concentrate on the radial rotation profile of the radiative zone. It is particularly difficult to extract, first because one needs to avoid the bias due to the surface latitudinal variation, secondly because the number of modes useful for this extraction is reduced and the radial modes contain no information on rotation. The basic expression that links the splitting $\delta\nu_{n,\ell,m}$ to the internal rotation is given by the following

expression (Thompson et al. 2003) and the *SOHO* results are shown in Figure 10(b)

$$\delta\nu_{n,\ell,m} = m \int_0^R \int_0^\pi K_\Omega^{n,\ell,m}(r,\theta)\Omega(r,\theta) r dr d\theta. \quad (13)$$

Another difficulty in this exercise is due to the error bars affected by the splitting values, as they result from a difference in frequencies. A priori, these splittings should not be directly affected by the subsurface effects but to be cautious, the present splittings are generally deduced from subseries of 72 days for the high degree splittings. Moreover, one needs to extract the rotation profiles at different latitudes to follow how the latitudinal effect evolves with radius.

The dedicated effort of the *SOHO* consortium has discovered evidence a rapid variation of the rotation just below the surface and the presence of a tachocline at the base of the convective zone (Spiegel & Zahn 1992; Thompson et al. 2003); the sudden suppression of the differential latitudinal rotation observed in the convective zone leads to solid body rotation in the whole radiative zone. For the core rotation and the rest of the radiative zone, specific studies have been pursued since the launch of *SOHO*. They show that the acoustic modes cannot extract any reliable information on the core below 0.2 $R_\odot$ (Couvidat et al. 2003a; Mathur et al. 2008; Eff-Darwich & Korzennik 2012). The GOLF acoustic mode splittings are given in table 1 of Couvidat et al. (2003a), and they contribute to a very flat rotation profile in the radiative zone outside the nuclear core. In that region, the analysis of longer series confirms that there is no latitudinal dependence except perhaps at 60 degrees, as was obtained recently by the most complete study of Eff-Darwich & Korzennik (2012). These authors perform a 2D internal solar rotation profile including latitudinal variation from the inversions of MDI 64 * 72 days, which means the analysis of more than 10 years of MDI data. If this fact is confirmed, it will be interesting to understand its origin.

In the core, the two global analyses of the GOLF data at low frequency discussed previously and the six dipole gravity splittings that vary from 860 nHz at higher frequency up to 900–950 nHz around 60 μHz largely exhibit greater values than the splittings of the low degree acoustic modes around 400 nHz (García et al. 2011). So an increase of the rotation in the solar core by a factor 5–7, as suggested in Turck-Chièze et al. (2004a); García et al. (2007), continues to be largely supported by the GOLF observations. Those observations will benefit from the very long observation of *SOHO* while waiting for new observations with improved detections (see the next section).

An increase of the rotation in the core has also been observed in more evolved solar-like stars (Bedding et al. 2011; Deheuvels et al. 2012). It is a natural and previously-modeled phenomenon (Pinsonneault et al. 1989) from a theoretical point of view, as the central rotation increases during the contraction phases and the transport of momentum during the main sequence is a slow process. But observations are crucial to give the order of magnitude of this rotation increase in the core because the hydrodynamical processes are associated with other processes like transport of momentum by internal waves generated at the base of the convective zone (Charbonnel & Talon 2005) or by transport of momentum due to the role of a potential fossil magnetic field (Eggenberger et al. 2005).

Recent detailed analyses of the transport of momentum by rotation (Turck-Chièze et al. 2010; Marques et al. 2012) show that the meridional circulation velocity is very low in the radiative zone during hydrogen burning. There is clear evidence of the role of the tachocline layers, at least having a barrier region of horizontal turbulent instability resulting from the two very different meridional circulation velocities in the radiative and convective zones. They also show that the descriptions of the pre-main sequence evolution and the end of hydrogen burning are certainly important parts of the evolution that need to be improved for a correct understanding of the hydrodynamical description of the radiative zones inside solar-like stars. The core rotation appears in the Sun and stars smaller than predicted by models with only transport of momentum by rotation, and the core rotation of the Sun appears as a relic of the first stage of the solar rotation at an epoch corresponding to the formation of planets. This stage certainly justifies a deeper study where magnetic activity would play a crucial

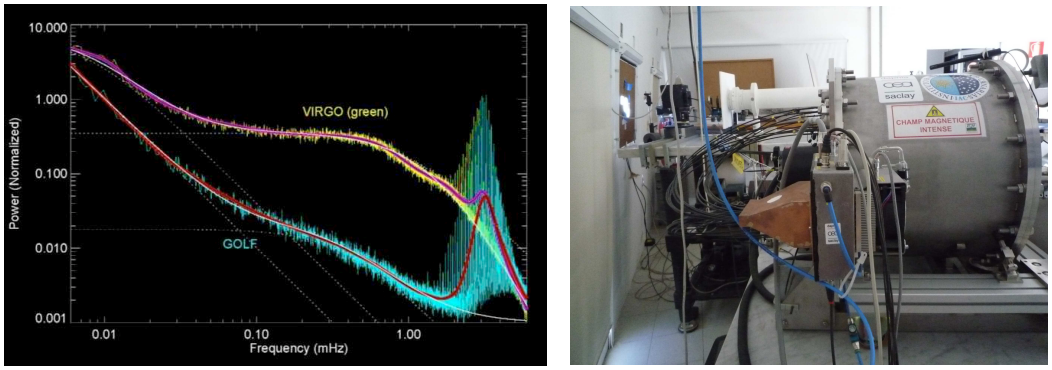

Fig. 11 *Left*: Comparison of the Fourier solar spectrum extracted from velocity (GOLF/*SOHO*) and intensity (VIRGO/*SOHO*) measurements. Derived from Stello et al. (2007). *Right*: The GOLF-NG prototype checked in a vacuum in the Saclay laboratory. From Turck-Chièze et al. (2008).

role, and even subsequently modeling the influence of gravity waves that also play a complementary role in eroding the rotation profile.

4.3 Detection of Solar Gravity Modes in Future Solar Missions

Progressing on the description of the radiative zone of the Sun and stars is certainly an objective of the following decades. It is justified by gaining a better understanding of the formation of stars and planets. The solar paradox could result from a very poor description of the first stage of evolution that could lead today to an incorrect time evolution of the luminosity during the first 50 Myrs (Turck-Chièze, Piau & Couvidat 2011b), but as these regions are difficult to check in young stars, current seismic observations represent a proven insight to check coming theoretical progress. A new effort in detection is also totally justified by the important role of stellar physics in more fundamental physics as shown in this review. This is why several studies have already been developed in parallel in recent years.

The left panel of Figure 11 compares the velocity and intensity spectra obtained simultaneously aboard *SOHO*. It shows the superiority of the first technique; the surface turbulence induces a noise in the low frequency part of the intensity spectrum that is reduced in velocity because the measurement of the velocity shift obtained where a spectral line (here sodium) is located, as said previously, around 500 km above the photosphere and is less sensitive to solar noise. It is also clear that measuring the velocity is better because it directly follows the phenomenon of oscillation $v = \mathrm{Re}[v_\mathrm{r}(r)Y_\ell^m(\theta,\phi)\mathrm{e}^{-i\omega t}]$.

4.3.1 GOLD, a space successor to GOLF and individual detection of neutrino fluxes

The space instrument GOLF, which was designed to improve our understanding of the solar core, has reached all its objectives. The small number of gravity modes detected by this instrument is due to their small amplitude and to the ageing of the instrument. One believes also that some of these modes are not as stable as previously believed along the period of observations due to the instability of the tachocline. Nevertheless, its fruitful production has largely demonstrated the ability of the used technique, illustrated by the left panel of Figure 11.

So a new prototype has been implemented to improve the capability of detecting low degree modes. The GOLF-NG concept is a 15 point resonant scattering spectrophotometer (instead of 2 or 4

in the case of GOLF), also observing the D1 sodium line and working in a vacuum to simulate space conditions (Turck-Chièze et al. 2006). The cell is placed in a varying permanent magnet (from 0 to 12 kG), and the scattered light, resulting from, alternatively, left and right circular polarized incident light, is extracted at eight different positions along the cell. Four outputs per position, connected to optical fibers by some circular lens, are placed around the cell, thus increasing the total photon counting rate compared to other existing instruments, in a total of 31 outputs. The main objective of this new concept is to reduce the instrumental and solar noises and consequently to increase the sensitivity to low signals at low and high frequency. The velocity signals are measured at different heights between 200 km and 800 km above the photosphere (at least four or five simultaneous heights that experience a different solar noise) to settle constraints on the variability of the emergence of the magnetic field and on the time evolution of the modes. All the required performances (increase the counting rate by factor of 10, low instrumental noise in comparison to the statistical noise) have been verified in the laboratory in thermal conditions as near as possible to space, by putting the instrument in a vacuum, see the right panel of Figure 11. A miniaturized version, called the GOLD (Global Oscillations of Low Degree modes) instrument must be prepared and launched into space for the next mission dedicated to monitoring the Sun.

In parallel, the capability to detect low energy neutrino fluxes and to separate the different contributors (see the previous review of Turck-Chièze & Couvidat (2011) for detailed information on future developments) will improve the statistics of each source of neutrinos and knowledge about the central temperature. A joint understanding of all the observables will definitively establish which processes act in the solar core and will even more strongly constrain the characteristics of dark matter and the relative importance of different processes.

4.3.2 The world formation flying mission for the Sun-Earth connection

In ESA's Cosmic Vision prospective, the concept of formation flying has appeared extremely well adapted for the next space-based solar mission, allowing long-term observations of the Sun (Turck-Chièze et al. 2009b). This concept allows numerous complementary probes of the Sun onboard and a permanent eclipse to obtain a good view of solar dynamics from the core to the corona, vision that has not yet been established. This approach will be useful for establishing the real impact of the Sun on the Earth over the long term through its varying activity. It would be nice to have for the first time a worldwide mission dedicated to space weather, space climate and fundamental physics.

5 SUMMARY AND CONCLUSIONS

This review shows the detailed interplay between solar-like stars and dark matter. Of course, the Sun is certainly not, a priori, the best object to look for dark matter. But we have shown that due to its unique place in our neighborhood and its privileged status as a laboratory of physics, the model of its radiative interior has been dramatically improved over the last decade thanks to both neutrinos and helioseismology. So the search for dark matter in its interior is totally justified. We have also demonstrated, by tables and figures, the remarkable coherence between the different observables that lead to an unprecedented vision of its deep interior, even if it is still incomplete. So we have deduced from the knowledge of its central density and temperature, independent constraints on the mass of WIMPs, disfavored to be below 12 GeV, and cross section interactions (see details).

Constraints on dark matter are strong but can still be improved by a detailed knowledge of the solar core below $0.05\,R_\odot$ through more detected gravity modes. A next generation of instruments and space missions are proposed. We have shown that good observation of the solar internal dynamics through the rotation profile has been obtained with the *SOHO* satellite, but one gets very few indications of a direct manifestation of the inner magnetic field except very near the surface.

Of course, other sources or manifestations of dark matter besides WIMPs must be searched for inside the Sun. We have mentioned the role of another candidate, the sterile neutrino, but we have

also argued that the effects of such a candidate will be difficult to separate from other redistributions of energy, such as kinetic, meridional or magnetic that are not yet definitively introduced in the structural equations, except for a first tentative step in Duez et al. (2010). In this context, the 3D simulations might be considered as a direction of progress in parallel to secular 1D models when they will be able to reproduce the dynamics of the real Sun.

In the present review, one has recalled that, beyond its exceptional study, the Sun is not the best star to look for dark matter; solar-like stars near the galaxy's center would certainly be better candidates for this search due to the density of dark matter in this region. The strong development of asteroseismic investigation of stellar populations with COROT (Miglio et al. 2012) is very promising. It will be extremely interesting to compare the seismic results of these two locations (our local neighborhood and the galactic center) to see if one can deduce some positive signature of this mysterious matter. Moreover, late stages of evolution have also been presented as promising cases through a new source of energy by annihilation of dark matter inside stars.

An armada of observational instruments will significantly increase the accuracy of solar and stellar data in the future, which will allow physicists to use the Sun and stars as tools to test some of the key ideas of modern fundamental physics, like new theories of gravitation, or inquire about the existence of new particles. Among other applications, we can mention the use of solar neutrinos and helioseismology data to test the validity of the experimental determination of Newton's Gravitational constant (Lopes & Silk 2003) or determine the validity of new gravitational theories proposed as an alternative to general relativity (Casanellas et al. 2012). The European satellite GAIA will also be a new important tool to better describe the dynamics of our galaxy.

Acknowledgements We express our deep gratitude to space agencies ESA and NASA for respectively building and maintaining the *SOHO* satellite and supporting its operation. We address special thanks to the French national agency CNES that has accompanied our efforts to extract the best results from the GOLF instrument since 1989 (construction, data analysis and interpretation) and to all our colleagues who have participated in different phases of this project and are quoted in this review. Some special thanks to P. Morel and J. Christensen-Dalsgaard for their efforts to build and deliver respectively the stellar code CESAM (we have also used the BINARY code initially written by Paszynski) and the oscillation code ADIPLS, which are extremely useful to the community and for the present results.

References

Aalseth, C. E., Barbeau, P. S., Colaresi, J., et al. 2011, Physical Review Letters, 107, 141301
Aharmim, B., Ahmed, S. N., Anthony, A. E., et al. 2010, Phys. Rev. C, 81, 055504
Ahmed, Z., Akerib, D. S., Arrenberg, S., et al. 2011, Physical Review Letters, 106, 131302
Archambault, S., Aubin, F., Auger, M., et al. 2009, Physics Letters B, 682, 185
Asplund, M., Grevesse, N., Sauval, A. J., & Scott, P. 2009, ARA&A, 47, 481
Bahcall, J. N., Serenelli, A. M., & Basu, S. 2005, ApJ, 621, L85
Basu, S., Chaplin, W. J., Elsworth, Y., New, R., & Serenelli, A. M. 2009, ApJ, 699, 1403
Bedding, T. R., Mosser, B., Huber, D., et al. 2011, Nature, 471, 608
Bernabei, R., Belli, P., Cappella, F., et al. 2008, European Physical Journal C, 56, 333
Bertello, L., Varadi, F., Ulrich, R. K., et al. 2000, ApJ, 537, L143
Bertone, G., Hooper, D., & Silk, J. 2005, Phys. Rep., 405, 279
Bouquet, A., & Salati, P. 1989, ApJ, 346, 284
Brown, A., Henry, S., Kraus, H., & McCabe, C. 2012, Phys. Rev. D, 85, 021301
Canuto, V. M., & Mazzitelli, I. 1991, ApJ, 370, 295
Casanellas, J., & Lopes, I. 2009, ApJ, 705, 135
Casanellas, J., & Lopes, I. 2011a, ApJ, 733, L51

Casanellas, J., & Lopes, I. 2011b, MNRAS, 410, 535
Casanellas, J., Pani, P., Lopes, I., & Cardoso, V. 2012, ApJ, 745, 15
Casas, R. A., Arias, V., Pena Ramírez, K., & Kroupa, P. 2012, arXiv:1205.5029 (MNRAS in press)
Catena, R., & Ullio, P. 2010, J. Cosmol. Astropart. Phys., 8, 4
Chaplin, W. J., Elsworth, Y., Miller, B. A., Verner, G. A., & New, R. 2007, ApJ, 659, 1749
Charbonnel, C., & Talon, S. 2005, Science, 309, 2189
Chieze, J.-P., Teyssier, R., & Alimi, J.-M. 1997, ApJ, 484, 40
Christensen-Dalsgaard, J. 2002, Rev. Mod. Phys., 74, 1073
Christensen-Dalsgaard, J. 2004, Sol. Phys., 220, 137
Aerts, C., Christensen-Dalsgaard, J., & Kurtz, D. W. 2010, Asteroseismology (Springer)
Christensen-Dalsgaard, J., & Berthomieu, G. 1991, Theory of Solar Oscillations, in Solar Interior and Atmosphere (Tucson, AZ: University of Arizona Press), 1991, 401
Claverie, A., Isaak, G. R., McLeod, C. P., van der Raay, H. B., & Cortes, T. R. 1979, Nature, 282, 591
Cohen, T., Phalen, D. J., Pierce, A., & Zurek, K. M. 2010, Phys. Rev. D, 82, 056001
Couvidat, S., García, R. A., Turck-Chièze, S., et al. 2003a, ApJ, 597, L77
Couvidat, S., Turck-Chièze, S., & Kosovichev, A. G. 2003b, ApJ, 599, 1434
Cox, A. N., Guzik, J. A., & Raby, S. 1990, ApJ, 353, 698
de Vega, H. J., & Sanchez, N. G. 2010, MNRAS, 404, 885
Dearborn, D., Griest, K., & Raffelt, G. 1991, ApJ, 368, 626
Deheuvels, S., Garcia, R. A., Chaplin, W. J., et al. 2012, arXiv:1206.3312
Del Nobile, E., Kouvaris, C., & Sannino, F. 2011, Phys. Rev. D, 84, 027301
Dintrans, B., Brandenburg, A., Nordlund, Å., & Stein, R. F. 2005, A&A, 438, 365
Domingo, V., Fleck, B., & Poland, A. I. 1995, Sol. Phys., 162, 1
Drukier, A. K., Freese, K., & Spergel, D. N. 1986, Phys. Rev. D, 33, 3495
Duez, V., Mathis, S., & Turck-Chièze, S. 2010, MNRAS, 402, 271
Eff-Darwich, A., & Korzennik, S. G. 2012, arXiv:1205.3143 (Sol. Phys. in press)
Eggenberger, P., Maeder, A., & Meynet, G. 2005, A&A, 440, L9
Farina, M., Pappadopulo, D., Strumia, A., & Volansky, T. 2011, J. Cosmol. Astropart. Phys., 11, 10
Felizardo, M., Girard, T. A., Morlat, T., et al. 2012, Physical Review Letters, 108, 201302
Feng, J. L. 2010, ARA&A, 48, 495
Fletcher, S. T., Broomhall, A.-M., Salabert, D., et al. 2010, ApJ, 718, L19
Frieman, J. A., Turner, M. S., & Huterer, D. 2008, ARA&A, 46, 385
Gabriel, A. H., Grec, G., Charra, J., et al. 1995, Sol. Phys., 162, 61
García, R. A., Régulo, C., Turck-Chièze, S., et al. 2001, Sol. Phys., 200, 361
García, R. A., Turck-Chièze, S., Boumier, P., et al. 2005, A&A, 442, 385
García, R. A., Turck-Chièze, S., Jiménez-Reyes, S. J., et al. 2007, Science, 316, 1591
Garcia, R. A., Jimenez, S. J., Mathur, S. et al., 2008, Astron. N., 329, 476
García, R. A., Salabert, D., Ballot, J., et al. 2011, Journal of Physics Conference Series, 271, 012046
Gelly, B., Lazrek, M., Grec, G., et al. 2002, A&A, 394, 285
Giraud-Heraud, Y., Kaplan, J., de Volnay, F. M., Tao, C., & Turck-Chieze, S. 1990, Sol. Phys., 128, 21
Giuliani, F. 2005, Physical Review Letters, 95, 101301
Gondolo, P., Edsjö, J., Ullio, P., et al. 2004, J. Cosmol. Astropart. Phys., 7, 8
Gould, A. 1987, ApJ, 321, 571
Grec, G., Fossat, E., & Pomerantz, M. 1980, Nature, 288, 541
Harvey, J. W., Hill, F., Hubbard, R. P., et al. 1996, Science, 272, 1284
Hooper, D., & Baltz, E. A. 2008, Annual Review of Nuclear and Particle Science, 58, 293
Hooper, D., & Kelso, C. 2011, Phys. Rev. D, 84, 083001
Ilie, C., Freese, K., Valluri, M., Iliev, I. T., & Shapiro, P. R. 2012, MNRAS, 422, 2164

Iocco, F., Taoso, M., Leclercq, F., & Meynet, G. 2012, Physical Review Letters, 108, 061301
Irwin, M., & Hatzidimitriou, D. 1995, MNRAS, 277, 1354
Jiménez, A., & García, R. A. 2009, ApJS, 184, 288
Jungman, G., Kamionkowski, M., & Griest, K. 1996, Phys. Rep., 267, 195
Kang, Z., Li, J., Li, T., Liu, T., & Yang, J. 2011, arXiv:1102.5644
Kaplan, J., Martin de Volnay, F., Tao, C., & Turck-Chieze, S. 1991, ApJ, 378, 315
Kaplan, D. E., Luty, M. A., & Zurek, K. M. 2009, Phys. Rev. D, 79, 115016
Komatsu, E., Smith, K. M., Dunkley, J., et al. 2011, ApJS, 192, 18
Kurylov, A., & Kamionkowski, M. 2004, Phys. Rev. D, 69, 063503
Lefebvre, S., Nghiem, P. A. P., & Turck-Chièze, S. 2009, ApJ, 690, 1272
Lopes, I., Casanellas, J., & Eugénio, D. 2011, Phys. Rev. D, 83, 063521
Lopes, I. P., & Gough, D. 2001, MNRAS, 322, 473
Lopes, I. P., & Silk, J. 2003, MNRAS, 341, 721
Lopes, I., & Silk, J. 2010a, Science, 330, 462
Lopes, I., & Silk, J. 2010b, ApJ, 722, L95
Lopes, I., & Silk, J. 2012, ApJ, 752, 129
Lopes, I., & Turck-Chieze, S. 1994, A&A, 290, 845
Marques, J. P., Goupil, M. J., Lebreton, Y. et al. 2012, A&A, submitted
Mathur, S., Turck-Chièze, S., Couvidat, S., & García, R. A. 2007, ApJ, 668, 594
Mathur, S., Eff-Darwich, A., García, R. A., & Turck-Chièze, S. 2008, A&A, 484, 517
Mention, G., Fechner, M., Lasserre, T., et al. 2011, Phys. Rev. D, 83, 073006
Miglio, A., Morel, T., Barbieri, M., et al. 2012, in European Physical Journal Web of Conferences, 19, Assembling the Puzzle of the Milky Way, Le Grand-Bornand, France, eds. C. Reylé, A. Robin, & M. Schultheis, 5012
Nordlund, Å., & Stein, R. F. 2000, in IAU Colloq. 176, The Impact of Large-Scale Surveys on Pulsating Star Research, Astronomical Society of the Pacific Conference Series, 203, eds. L. Szabados, & D. Kurtz, 362
Passos, D., Brandão, S., & Lopes, I. 2007, Advances in Space Research, 40, 990
Piau, L., Collet, R., Morel, P., & Turck-Chièze, S. 2012, A&A, in preparation
Pinsonneault, M. H., Kawaler, S. D., Sofia, S., & Demarque, P. 1989, ApJ, 338, 424
Press, W. H., & Spergel, D. N. 1985, ApJ, 296, 679
Provost, J., & Berthomieu, G. 1986, A&A, 165, 218
Provost, J., Berthomieu, G., & Morel, P. 2000, A&A, 353, 775
Rhodes, E. J., Jr., Kosovichev, A. G., Schou, J., Scherrer, P. H., & Reiter, J. 1997, Sol. Phys., 175, 287
Ricotti, M., & Gould, A. 2009, ApJ, 707, 979
Rosenthal, C. S., Christensen-Dalsgaard, J., Nordlund, Å., Stein, R. F., & Trampedach, R. 1999, A&A, 351, 689
Salabert, D., García, R. A., Pallé, P. L., & Jiménez-Reyes, S. J. 2009, A&A, 504, L1
Salati, P., & Silk, J. 1989, ApJ, 338, 24
Scherrer, P. H., Bogart, R. S., Bush, R. I., et al. 1995, Sol. Phys., 162, 129
Scott, P., Fairbairn, M., & Edsjö, J. 2009, MNRAS, 394, 82
Scott, P., Venkatesan, A., Roebber, E., et al. 2011, ApJ, 742, 129
Simoniello, R., Finsterle, W., Salabert, D., et al. 2012, A&A, 539, A135
Spergel, D. N., & Press, W. H. 1985, ApJ, 294, 663
Spiegel, E. A., & Zahn, J.-P. 1992, A&A, 265, 106
Springel, V., White, S. D. M., Jenkins, A., et al. 2005, Nature, 435, 629
Stello, D., Kjeldsen, H., & Bedding, T. R. 2007, in Astronomical Society of the Pacific Conference Series, 366, Transiting Extrapolar Planets Workshop, eds. C. Afonso, D. Weldrake, & T. Henning, 247
Taoso, M., Iocco, F., Meynet, G., Bertone, G., & Eggenberger, P. 2010, Phys. Rev. D, 82, 083509
Tassoul, M. 1980, ApJS, 43, 469

Teyssier, R. 2002, A&A, 385, 337
Teyssier, R., Pires, S., Prunet, S., et al. 2009, A&A, 497, 335
Thompson, M. J., Christensen-Dalsgaard, J., Miesch, M. S., & Toomre, J. 2003, ARA&A, 41, 599
Turck-Chièze, S., & Couvidat, S. 2011, Reports on Progress in Physics, 74, 086901
Turck-Chièze, S., & Lopes, I. 1993, ApJ, 408, 367
Turck-Chièze, S., Däppen, W., Fossat, E., et al. 1993, Phys. Rep., 230, 57
Turck-Chièze, S., Basu, S., Brun, A. S., et al. 1997, Sol. Phys., 175, 247
Turck-Chièze, S., Couvidat, S., Kosovichev, A. G., et al. 2001, ApJ, 555, L69
Turck-Chièze, S., García, R. A., Couvidat, S., et al. 2004a, ApJ, 608, 610
Turck-Chièze, S., Couvidat, S., Piau, L., et al. 2004b, Physical Review Letters, 93, 211102
Turck-Chièze, S., Carton, P.-H., Ballot, J., et al. 2006, Advances in Space Research, 38, 1812
Turck-Chièze, S., Carton, P. H., Mathur, S., et al. 2008, Astronomische Nachrichten, 329, 521
Turck-Chièze, S., Delahaye, F., Gilles, D., Loisel, G., & Piau, L. 2009a, High Energy Density Physics, 5, 132
Turck-Chièze, S., Lamy, P., Carr, C., et al. 2009b, Experimental Astronomy, 23, 1017
Turck-Chièze, S., Palacios, A., Marques, J. P., & Nghiem, P. A. P. 2010, ApJ, 715, 1539
Turck-Chièze, S., Piau, L., & Couvidat, S. 2011, ApJ, 731, L29
Turck-Chièze, S., Piau, L., & Couvidat, S. 2011, ApJ, 731, L29
Turck-Chièze, S., García, R. A., Lopes, I., et al. 2012, ApJ, 746, L12
Turner, M. S. 1986, Phys. Rev. D, 33, 889
Unno, W., Osaki, Y., Ando, H., Saio, H., & Shibahashi, H. 1989, Nonradial Oscillations of Stars (University of Tokyo Press)
Verner, G. A., Elsworth, Y., Chaplin, W. J., et al. 2011, MNRAS, 415, 3539
Vorontsov, S. V. 1991, Soviet Ast., 35, 400
Willman, B., Blanton, M. R., West, A. A., et al. 2005, AJ, 129, 2692
Xenon100 Collaboration, Aprile, E., Arisaka, K., et al. 2012, Astroparticle Physics, 35, 573